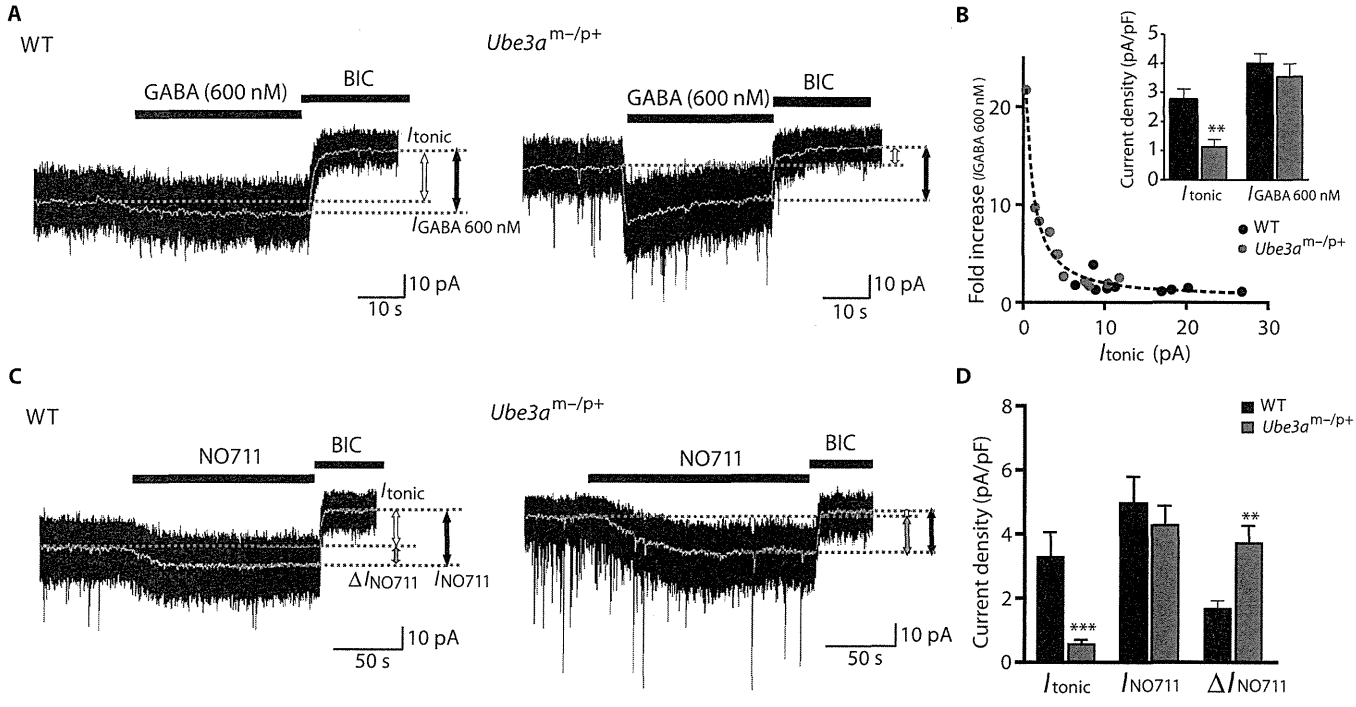

Fig. 2. GABA decreases due to increased GAT1 activity underlie the decreased tonic inhibition found in *Ube3a*$^{m-/p+}$ mice. (**A**) Representative traces showing the effects of GABA (600 nM) application on base holding currents. Each baseline is indicated by a dotted line. Tonic holding currents induced by endogenous (I_{tonic}) and exogenous GABA ($I_{GABA\ 600\ nM}$) are indicated by thick white and black vertical arrows, respectively. (**B**) The fold increase of $I_{GABA\ 600\ nM}$ against I_{tonic} is plotted for each cerebellar granule cell from WT (black circle) and *Ube3a*$^{m-/p+}$ (red circle) mice. The fitted curve (dotted line) was integrally calculated from WT and *Ube3a*$^{m-/p+}$ mice with a Hill equation. The inset graph shows a comparison of current densities in WT (n = 9, black) and *Ube3a*$^{m-/p+}$ (n = 11, red) mice. (**C**) Representative current traces showing the effect of NO711 on base holding currents. I_{tonic}, NO711-induced base holding currents (I_{NO711}), and the change in holding currents (ΔI_{NO711}) are indicated by thick white, black, and gray vertical arrows, respectively. (**D**) Comparison of current densities in WT (n = 7, black) and *Ube3a*$^{m-/p+}$ (n = 9, red) mice. $^{**}P < 0.01$, $^{***}P < 0.001$, unpaired t test. Data are means ± SEM.

on tonic inhibition using a GAT1 inhibitor, NO711 (40 μM). Tonic holding currents showed larger amplitudes after bath application of NO711 (I_{NO711}) than before (I_{tonic}) in all evaluated cells. Although the increase in tonic currents induced by NO711 (ΔI_{NO711}) was larger in *Ube3a*$^{m-/p+}$ mice than in wild-type mice, I_{tonic} itself was significantly decreased ($P < 0.001$; Fig. 2, C and D). Consequently, I_{NO711} was not different between *Ube3a*$^{m-/p+}$ and wild-type mice ($P = 0.51$; Fig. 2D), suggesting that excessive uptake of GABA via GAT1 could give rise to decreased tonic inhibition in *Ube3a*$^{m-/p+}$ mice. Indeed, GAT1 protein concentrations in the cerebellum of *Ube3a*$^{m-/p+}$ mice were significantly elevated at P32 ($P < 0.05$; Fig. 3, A and B), and a tendency toward an elevation was seen in 5-month-old mice (fig. S4). In contrast, expression of $GABA_A$ receptor subunit α6 did not differ between wild-type and *Ube3a*$^{m-/p+}$ mice (Fig. 3, A and B).

Ube3a binds to GAT1 and regulates its stability

Because GAT1 mRNA expression did not increase in *Ube3a*$^{m-/p+}$ mice [GAT1/GAPDH (glyceraldehyde-3-phosphate dehydrogenase): wild-type, 1.00 ± 0.22, n = 3, versus *Ube3a*$^{m-/p+}$, 1.13 ± 0.28, n = 3; P = 0.65], aberrant posttranscriptional modifications relevant to Ube3a deficiency seemed a likely mechanism for increased GAT1 activity. To test this, we performed an in vitro degradation assay (*25*, *26*) using cerebellar lysates and found that GAT1 protein rapidly degraded in cerebellar lysates derived from wild-type mice, but was stable in those derived from *Ube3a*$^{m-/p+}$ mice (Fig. 3, C and D). This suggests that Ube3a may be involved in degradation of GAT1 in the mouse cerebellum.

We next investigated whether GAT1 interacts with Ube3a in intact cells. Human embryonic kidney (HEK) 293 cells were transfected with or without FLAG-GAT1 and/or Myc-Ube3a. Myc-Ube3a was immunoprecipitated with anti-Myc antibody from whole-cell lysates after immunoblotting with anti-FLAG antibody. FLAG-GAT1 was coprecipitated with Myc-Ube3a (Fig. 3E, middle and bottom panels, lane 1 versus lane 2). Alternatively, FLAG-GAT1 was immunoprecipitated with anti-FLAG antibody from whole-cell lysates after immunoblotting with anti-Myc antibody. Myc-Ube3a was coprecipitated with FLAG-GAT1 (Fig. 3E, top panel, lane 4). GAT1 binding to Myc-Ube3a was detected as indicated by the arrow in Fig. 3E (middle and bottom panels, lane 2). Simultaneously, immunoblot analysis with anti-FLAG or anti-GAT1 confirmed oligomerized GAT1 protein, which was detected as a smear. Our results are consistent with those of previous reports that exogenously overexpressed GAT1 protein tends to be oligomerized in cultured cells (*27*, *28*). Because denaturing gels were used, these results do not directly show that Ube3a binds to monomeric GAT1 in intact cells but do suggest a potential interaction between Ube3a and GAT1.

To investigate whether endogenous Ube3a can bind to GAT1 in mouse cerebellum, we performed immunoprecipitation after immunoblotting

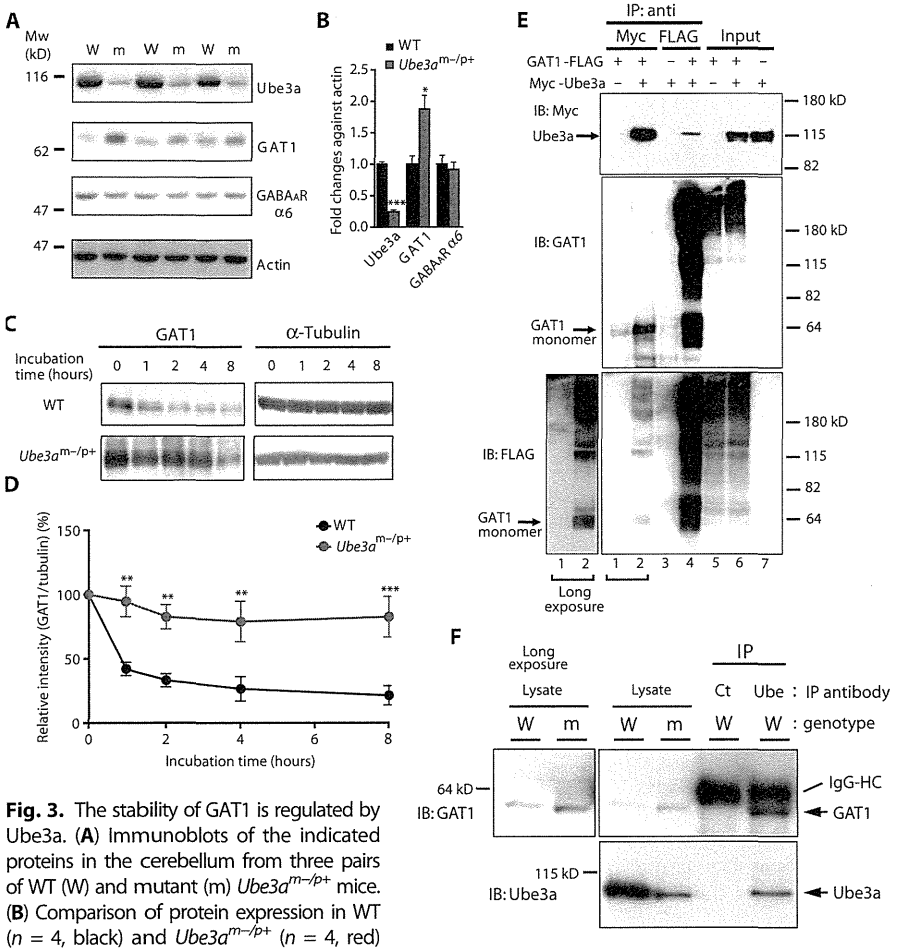

Fig. 3. The stability of GAT1 is regulated by Ube3a. (**A**) Immunoblots of the indicated proteins in the cerebellum from three pairs of WT (W) and mutant (m) *Ube3a*$^{m-/p+}$ mice. (**B**) Comparison of protein expression in WT (n = 4, black) and *Ube3a*$^{m-/p+}$ (n = 4, red) mice. *P < 0.05, ***P < 0.001, unpaired t test. (**C**) Representative immunoblots of an in vitro degradation assay for GAT1. (**D**) Percentage of GAT1 remaining after the indicated incubation times in WT (n = 4, black) and *Ube3a*$^{m-/p+}$ (n = 4, red) mice. The percentage of GAT1 protein was normalized to α-tubulin and calculated as the mean ± SEM from four mice. **P < 0.01, ***P < 0.001 by post hoc analysis for the genotypic group comparison after a two-way repeated-measures analysis of variance (ANOVA). (**E**) Interaction between GAT1 and Ube3a in HEK293 cells transfected with or without FLAG-GAT1 and/or Myc-Ube3a. (**F**) Interaction of endogenous GAT1 and Ube3a in the mouse cerebellum. Ube3a protein was immunoprecipitated (IP) with anti-Ube3a (Ube) or control immunoglobulin G (IgG) (Ct) antibody from lysates prepared from WT mouse cerebellum. Then, the immunoprecipitates and the original cell lysates prepared from WT and mutant *Ube3a*$^{m-/p+}$ mice were separated by SDS–polyacrylamide gel electrophoresis (SDS-PAGE), followed by immunoblotting (IB) with either anti-GAT1 or anti-Ube3a antibody. HC, heavy chain.

assays using lysates prepared with immunoprecipitation lysis buffer containing the proteasome inhibitor MG132 from wild-type mouse cerebellum (see Supplementary Materials and Methods). As shown in Fig. 3F, endogenous GAT1 was detected in the immunoprecipitate with anti-Ube3a antibody, but not with control IgG. This result indicates that endogenous Ube3a binds to endogenous GAT1 in mouse cerebellum.

Electrophysiological cerebellar dysfunction in *Ube3a*$^{m-/p+}$ mice in vitro is due to decreased tonic inhibition

Tonic $GABA_A$ receptor–mediated conductance can control the excitability of cerebellar granule cells by decreasing total membrane input resistance (*29*–*31*), a phenomenon referred to as shunting inhibition. However, other membrane conductances such as leak K^+ currents (*32*) may compensate for persistently low input resistance. To determine whether cerebellar granule cell excitability is altered by the decreased tonic inhibition observed in *Ube3a*$^{m-/p+}$ mice, we evaluated resting and firing membrane properties using whole-cell current-clamp recordings. Cerebellar granule cells of *Ube3a*$^{m-/p+}$ mice showed higher input resistance (table S1) and required lower current injection to reach action potential threshold (Fig. 4A and table S1). The relationship between firing rate and the injected current shifted to the left until the injected currents reached about 20 pA, indicating that lower current injections resulted in higher firing rates in *Ube3a*$^{m-/p+}$ mice (Fig. 4B). In contrast, the current-voltage relationships for the leak conductances and input resistances in the presence of BIC, strychnine, 6-cyano-7-nitroquinoxaline-2,3-dione (CNQX), D-(−)-2-amino-5-phosphonovaleric acid (AP5), and tetrodotoxin (TTX) were not significantly different (leak conductance: P = 0.98, Kolmogorov-Smirnov test, Fig. 4C; input resistance: P = 0.82, unpaired t test, table S1), indicating a lack of adaptive regulation for neuronal excitability. Bath application of low-dose 4,5,6,7-tetrahydroisothiazolo-[5,4-c]pyridin-3-ol (THIP; 500 nM), a selective agonist for extrasynaptic $GABA_A$ receptors containing the δ subunit (*33*), significantly increased tonic holding currents (from 0.84 ± 0.35 to 4.26 ± 0.6 pA/pF; P < 0.01, paired t test; n = 4) and reduced the excitability (Fig. 4D and fig. S5D) of *Ube3a*$^{m-/p+}$ cerebellar granule cells. THIP (500 nM) also increased the tonic holding currents and tempered the excitability in wild-type mice, but the efficacy was lower than that in *Ube3a*$^{m-/p+}$ mice (fig. S5). These findings demonstrate that the membrane excitability of cerebellar granule cells increased to near action potential threshold due to the decreased tonic inhibition in *Ube3a*$^{m-/p+}$ mice.

We also found that cerebellar granule cells of *Ube3a*$^{m-/p+}$ mice exhibited spike rate adaptation (Fig. 4, A and B) corresponding to the decreased after-hyperpolarization (table S1). The spike rate adaptation was still observed in the presence of THIP (Fig. 4D). The half width and rise time of action potentials were also increased in cerebellar granule cells of *Ube3a*$^{m-/p+}$ mice (table S1). Together, these results suggest that intrinsic firing properties are altered by Ube3a deficiency in cerebellar granule cells.

Purkinje cells are the only output cells in the cerebellar cortex. To determine whether the decreased tonic inhibition in cerebellar granule cells could be attributed to cerebellar dysfunction, we next evaluated the spontaneous firing properties of Purkinje cells in acutely prepared

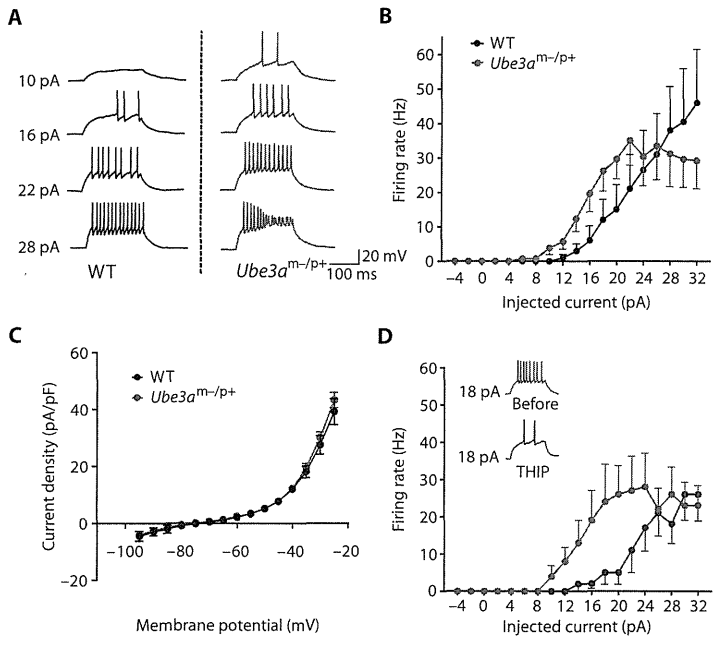

Fig. 4. Decreased tonic inhibition increases cerebellar granule cell membrane excitability in *Ube3a*$^{m-/p+}$ mice. (**A**) Representative responses of cerebellar granule cells (voltage held at −65 mV) to current injection in WT and *Ube3a*$^{m-/p+}$ mice. (**B**) Averaged input-output relationship of cerebellar granule cells from WT (n = 10) and *Ube3a*$^{m-/p+}$ (n = 12) mice. (**C**) Averaged current-voltage relationship for leak K^+ conductance in cerebellar granule cells from WT (n = 10) and *Ube3a*$^{m-/p+}$ (n = 10) mice. (**D**) Averaged input-output relationship in cerebellar granule cells (n = 5) from *Ube3a*$^{m-/p+}$ mice in the absence (red trace) or presence of THIP (blue trace). Inset traces show representative responses of cerebellar granule cells (voltage held at −65 mV) to 18-pA current injection in the absence (red) or presence of THIP (blue). All data are means ± SEM.

cerebellar brain slices with extracellular single-unit recordings. With the exception of three Purkinje cells in *Ube3a*$^{m-/p+}$ mice that showed a characteristic tonic silent pattern, all successfully recorded Purkinje cells from wild-type and *Ube3a*$^{m-/p+}$ mice showed either tonic or trimodal (*34*) firing patterns (Fig. 5A). Although only half of the wild-type Purkinje cells presented a tonic pattern [as shown in previous reports (*34*, *35*)], the proportion reached 80% in *Ube3a*$^{m-/p+}$ Purkinje cells (Fig. 5B), with only 2 of 25 cells displaying the trimodal pattern. The firing pattern was consistent in each cell throughout recordings lasting over 5 min. However, bath application of THIP (500 nM) altered the firing pattern from tonic to trimodal in four of five Purkinje cells in *Ube3a*$^{m-/p+}$ mice (Fig. 5C). The same change was observed in the tonic firing pattern in wild-type mice (two of two cells; fig. S6A), but the trimodal pattern in wild-type mice was not altered by THIP (two of two cells; fig. S6B). It has been shown that intrinsic Purkinje cell firing patterns show a trimodal pattern, because blockage of excitatory and inhibitory inputs changed the firing pattern from tonic to trimodal (*34*). THIP increased tonic holding currents in cerebellar granule cells (see above) but not in Purkinje cells from *Ube3a*$^{m-/p+}$ mice (Fig. 5D). Thus, decreased tonic inhibition leads to increases in spontaneous synaptic inputs from cerebellar granule cells to Purkinje cells and can account for the abnormally high proportion of Purkinje cells displaying tonic firing patterns in *Ube3a*$^{m-/p+}$ mice.

The Purkinje cell firing rate and the coefficient of variance of the interspike intervals during tonic firing did not differ between wild-type and *Ube3a*$^{m-/p+}$ mice (fig. S7). However, Ube3a deficiency could affect the intrinsic firing properties of Purkinje cells as witnessed by the characteristic tonic silent pattern that was not affected by THIP (n = 2).

THIP can partially rescue the cerebellar dysfunction in vivo

Previous studies have reported that hind paw width and stride in *Ube3a*$^{m-/p+}$ mice were larger than (*36*, *37*) or similar to those in wild-type mice (*2*). In our evaluation, they were not significantly different (P = 0.44 and 0.73, respectively; Fig. 6, A and B). However, gait analysis revealed that the angle between the left and right hind paw axes (paw abduction) was significantly larger in *Ube3a*$^{m-/p+}$ mice (P < 0.001; Fig. 6, A and B). To discern the contribution of decreased I_{tonic} to cerebellar ataxia, we evaluated the effects of THIP in vivo in mice aged 3 to 5 months. Intraperitoneal injection of THIP (2.5 mg/kg) reduced the hind paw abduction in *Ube3a*$^{m-/p+}$ mice without affecting the width or stride (Fig. 6, C to E). In contrast, THIP (2.5 mg/kg) did not alter gait parameters in wild-type mice (fig. S8, A and B).

When mice were held by their tails (tail suspension test), *Ube3a*$^{m-/p+}$ mice (*37*) as well as mice of other strains presenting cerebellar ataxia (*23*, *38*) show a clasping reflex, represented by forelimb clasping and flexion to the body. We evaluated the clasping behavior with a previously reported scoring method (*38*) and by measuring the forelimb angle against the body axis viewed laterally. Scoring was conducted blindly, with evaluators unaware of the mouse genotypes or the drugs used. All *Ube3a*$^{m-/p+}$ mice showed a mild to moderate clasping reflex (fig. S9A) and smaller forelimb angles compared with wild-type mice due to forelimb flexion (Fig. 6, F and G). Five of seven *Ube3a*$^{m-/p+}$ mice showed improved clasping reflexes after treatment with THIP (2.5 mg/kg) intraperitoneally (fig. S9B). THIP also significantly increased the forelimb angles in *Ube3a*$^{m-/p+}$ mice (P < 0.01; Fig. 6, H and I, and movie S1) but not in wild-type mice (P = 0.56; fig. S8C).

Consistent with previous findings, time spent on an accelerating rotarod was shorter in *Ube3a*$^{m-/p+}$ mice than in wild-type mice (Fig. 7A). This was improved significantly by THIP at 1.25 mg/kg (P < 0.05) but not significantly by THIP at 2.5 mg/kg (P = 0.20; Fig. 7B). Comparison of this effect between wild-type and *Ube3a*$^{m-/p+}$ mice revealed that THIP (1.25 mg/kg) was specifically effective for *Ube3a*$^{m-/p+}$ mice but not for wild-type mice (Fig. 7C and fig. S8D).

THIP concentrations in the rat brain have been reported to reach up to 700 nM with a subcutaneous administration of 2.5 mg/kg (*39*), a concentration much lower than that needed to activate nonspecific $GABA_A$ receptors that lack the δ subunit (*33*). Therefore, these in vivo analyses demonstrate that decreased tonic inhibition in cerebellar granule cells underlies the cerebellar dysfunction in *Ube3a*$^{m-/p+}$ mice.

DISCUSSION

Here, we have demonstrated that cerebellar granule cells in a mouse model of Angelman syndrome exhibit decreased tonic inhibition and aberrant membrane excitability. Pharmacological enhancement of

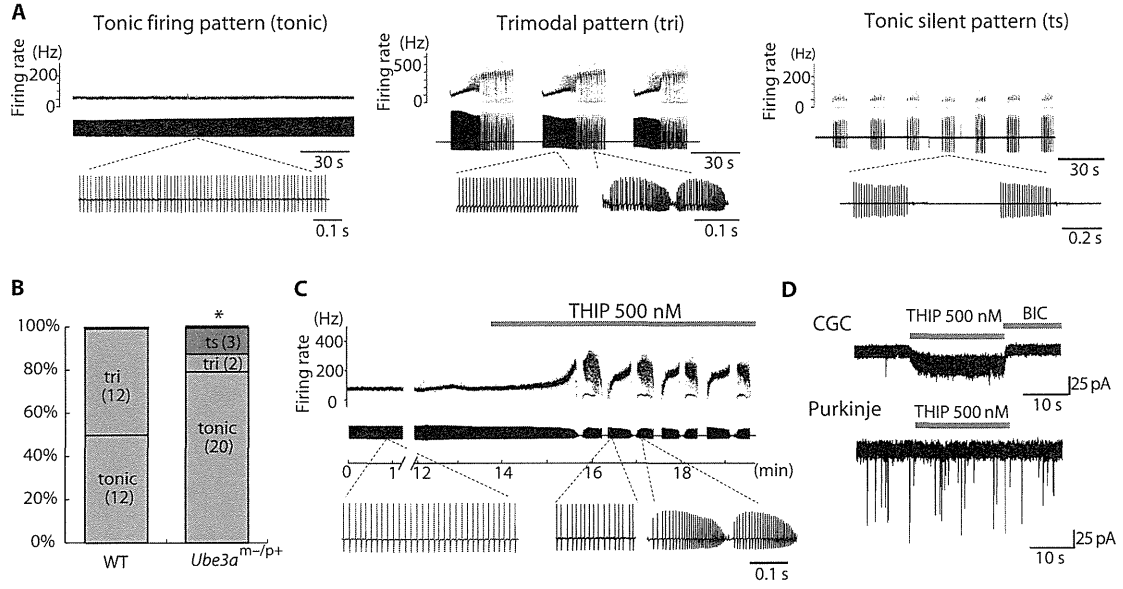

Fig. 5. Administration of THIP alters Purkinje cell firing patterns in *Ube3a*$^{m-/p+}$ mice. (**A**) Three representative firing patterns observed in Purkinje cells using single-unit recordings. Firing rates (upper traces), waveforms (middle traces), and expanded waveforms (bottom traces) are plotted. Left panel: continuous, stable firing rate [tonic pattern (tonic)]; middle panel: recurrence of tonic and burst-like firing interspersed with silent periods [trimodal pattern (tri)]; right panel: short, stable firing interrupted by repetitive pause and followed by a silent period [tonic silent pattern (ts)]. (**B**) Proportion of each firing pattern in WT (n = 24) and *Ube3a*$^{m-/p+}$ (n = 25) mice. The number of cells is indicated in each column. The tonic-pattern ratio was compared between WT and *Ube3a*$^{m-/p+}$ mice with a χ^2 test. *$P < 0.05$. (**C**) Representative traces illustrating the change in firing pattern caused by bath application of THIP (500 nM) in a brain slice from a *Ube3a*$^{m-/p+}$ mouse. (**D**) Representative current traces of cerebellar granule cells (CGC) and Purkinje cells from *Ube3a*$^{m-/p+}$ mice showing the effect of focal THIP (500 nM) application on base holding currents. All data are means ± SEM.

tonic inhibition reduces motor dysfunction in these mice, suggesting that decreased tonic inhibition is an important mechanism underlying the movement disorder in Angelman syndrome. Furthermore, we have shown that Ube3a deficiency reduces the degradation of GAT1, and that this, in turn, decreases tonic inhibition.

Extrasynaptic $GABA_A$ receptor–mediated tonic inhibition was first identified in rat cerebellar granule cells (*40*), and its pharmacological manipulation has been shown to regulate cerebellar granule cell (*29*–*31*) and Purkinje cell (*30*) excitability. However, the effects of long-term deficiencies in tonic inhibition on cerebellar function have not been fully understood because extrasynaptic $GABA_A$ receptor–null mutant mice did not show ataxia as a result of compensatory increases in potassium conductance in cerebellar granule cells (*32*). We have shown that decreased I_{tonic} resulting from the reduction in ambient GABA concentrations causes cerebellar dysfunction in *Ube3a*$^{m-/p+}$ mice. Because cerebellar ataxia was successfully improved by administration of an extrasynaptic $GABA_A$ receptor–selective agonist, THIP, our results highlight the importance of ambient GABA regulation in maintaining cerebellar function by regulating I_{tonic} and cerebellar granule cell excitability.

More specifically, we have discovered that Ube3a regulates tonic inhibition by controlling the degradation of GAT1. Although GAT1 can be expressed in astrocytes as well as neurons (*22*), Ube3a is expressed exclusively in neurons (*18*, *24*). Therefore, our findings suggest the importance of neuronal GAT1 in the regulation of ambient GABA concentrations in the cerebellar granule cell layer. Neuronal GAT1 may also affect sIPSCs by decreasing decay time (*23*); however, our evidence showing that sIPSCs were not altered in cerebellar granule cells from *Ube3a*$^{m-/p+}$ mice is in agreement with previous data (*20*). Given that inhibitory input onto cerebellar granule cells shifts from phasic to tonic along with development (*19*), it is conceivable that the dominant effect of GAT1 is exclusively on tonic inhibition.

Our in vivo studies using THIP represent a potential therapeutic strategy for Angelman syndrome by compensating for the decreased tonic inhibition. Tiagabine, an antiepileptic drug that inhibits GAT1, might also be effective for similar reasons. However, for the clinical administration of these drugs, the range of therapeutic doses should be considered carefully because excessive tonic inhibition can also induce neuronal dysfunction (*16*, *17*). The regulatory mechanisms for ambient GABA in the brain differ from region to region. For example, GAT1 in the rat thalamus is exclusively expressed in astrocytes (*41*), which implies unchanged tonic inhibition in the thalamus of Angelman syndrome individuals. Therefore, a therapeutic increase in tonic inhibition may adversely affect the functions of the thalamo-cortical network. This implication is supported by a clinical report of vigabatrin-induced seizure aggravation in Angelman syndrome (*42*). Whereas THIP (2.5 mg/kg) did not affect rotarod performance in wild-type mice in line with the findings of a previous report (*43*), a recent study reported reduced locomotor activity in wild-type mice after administration of THIP (2.0 mg/kg) (*44*). Thus, possible adverse effects of THIP (2.5 mg/kg) could mask improvements in cerebellar ataxia in *Ube3a*$^{m-/p+}$ mice, resulting in unchanged rotarod performance with the higher dose of THIP. Whereas tiagabine shows higher affinity in the thalamus than the cerebellar granule cell layer (*45*), THIP displays the opposite pattern (*46*). Thus, we propose that low doses of THIP potentially may be an effective treatment for the cerebellar ataxia in Angelman syndrome.

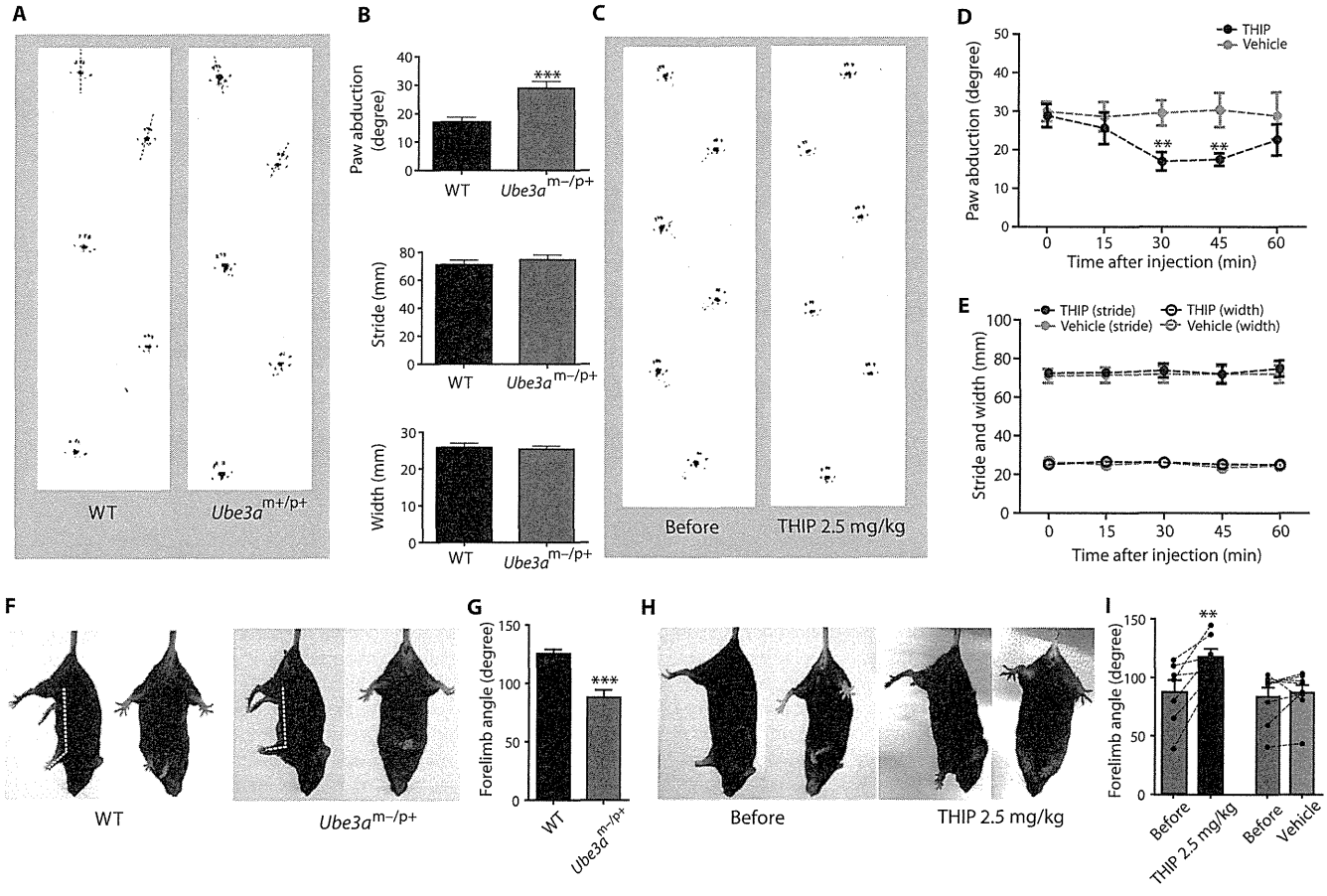

Fig. 6. Administration of THIP improves ataxia in *Ube3a*$^{m-/p+}$ mice. (**A** and **B**) Representative footprint traces (A) and comparison of each parameter (B) in WT (n = 10) and *Ube3a*$^{m-/p+}$ (n = 11) mice. (**C**) Representative footprint traces before and 30 min after administration of THIP (2.5 mg/kg) in *Ube3a*$^{m-/p+}$ mice. (**D**) Changes over time of paw abduction angles after injection of THIP (blue) or saline (gray) in *Ube3a*$^{m-/p+}$ mice. (**E**) Analyses over time of stride length (filled circles) and base width (empty circles) after administering THIP (blue) or saline (gray) in *Ube3a*$^{m-/p+}$ mice. (**F**) Representative limb postures responding to tail suspension in WT and *Ube3a*$^{m-/p+}$ mice. (**G**) Comparison of the forelimb angles against body axes in the tail suspension test. Angles were evaluated from a side view as indicated by dotted lines in (F) (WT, n = 14; *Ube3a*$^{m-/p+}$, n = 15). (**H**) Representative responses to tail suspension before and 40 min after THIP (2.5 mg/kg) administration. (**I**) Effects of THIP and saline on forelimb angles in the tail suspension test. $^{**}P < 0.01$, $^{***}P < 0.001$. Unpaired t test (B and G), one-way repeated-measures ANOVA (D and E), or paired t tests (I) were performed. Data are means ± SEM.

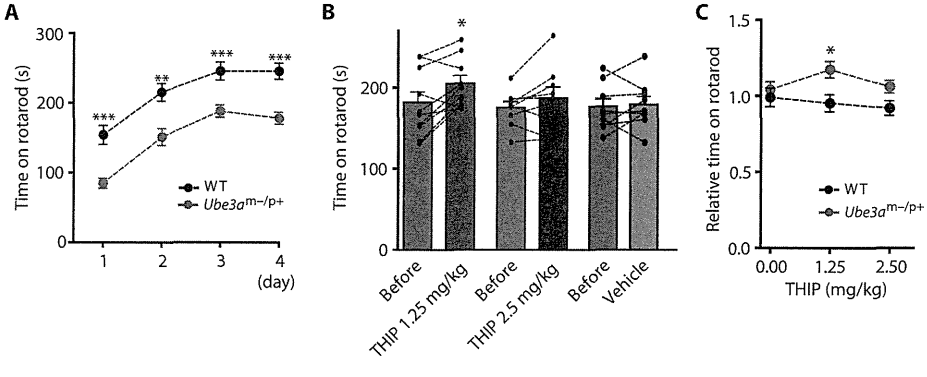

Fig. 7. Administration of THIP improves rotarod scores in *Ube3a*$^{m-/p+}$ mice. (**A**) Comparison of time spent on a rotarod between WT (black) and *Ube3a*$^{m-/p+}$ (red) mice. (**B**) Effects of THIP (1.25 or 2.5 mg/kg) or saline on time spent on a rotarod in *Ube3a*$^{m-/p+}$ mice. (**C**) Comparison of the dose-dependent effects of THIP on time spent on a rotarod in WT (black) and *Ube3a*$^{m-/p+}$ (red) mice. The amount of time 30 min after an injection was normalized to the time before the injection. $^{*}P < 0.05$, $^{**}P < 0.01$, $^{***}P < 0.001$. Two-way repeated-measures ANOVA (A and C) or paired t tests (B) were performed. Data are means ± SEM.

Partial rescue by in vivo THIP administration in *Ube3a*$^{m-/p+}$ mice suggests that other mechanisms, such as dysfunction of the nigrostriatal pathway (*37*), could be involved in the motor dysfunction in Angelman syndrome. We also observed THIP-insensitive aberrant firing properties in both cerebellar granule cells and Purkinje cells from *Ube3a*$^{m-/p+}$ mice, the mechanisms of which are still being elucidated. Increased Na/K-ATPase (adenosine triphosphatase) and lower resting membrane potentials were recently shown in CA1 hippocampal neurons from *Ube3a*$^{m-/p+}$ mice (*47*). The same deregulation might explain the tonic-silent pattern of Purkinje cell firing in *Ube3a*$^{m-/p+}$ mice.

The spike rate adaptation with lower amplitude after hyperpolarization of cerebellar granule cells might result from deactivation of large-conductance K^+ (BK) channels (*48*) due to the decreased activity of calcium/calmodulin-dependent protein kinase II in *Ube3a*$^{m-/p+}$ mice (*5*). Previous in vivo analysis in *Ube3a*$^{m-/p+}$ mice showed that aberrant Purkinje cell firing consisted of the increased frequency and rhythmicity of simple spikes (*49*). Because simple spikes are modulated by parallel fiber input, our observation of lower threshold currents for eliciting action potentials and reduced repetitive firing in cerebellar granule cells in vitro can explain the results of in vivo Purkinje cell firing analysis. Decreased burst firing of cerebellar granule cells due to reduced repetitive firing can cause the higher rhythmicity of simple spikes. Because reduced ongoing firing due to I_{tonic} and intrinsic bursting properties are both critical for shaping a high signal-to-noise ratio of information flow via cerebellar granule cells in vivo (*31*), the collapse of this regulation might synergistically aggregate cerebellar dysfunction in *Ube3a*$^{m-/p+}$ mice.

Because neuronal GAT1 is widely expressed in the CNS, its attenuated degradation could contribute to other symptoms of Angelman syndrome (*4*) and to the phenotype-genotype correlation relevant to the hemizygosity of $GABA_A$ receptor subunit genes such as α5 and β3 (*11*, *12*). Although the number of $GABA_A$ benzodiazepine-binding receptors did not decrease (*50*), the relative expression of β3 and α5 was reduced in Angelman syndrome patients lacking these genes (*51*). Because β3 is a major component of extrasynaptic $GABA_A$ receptors (*15*) and α5 is primarily expressed extrasynaptically in the hippocampus (*52*), tonic inhibition may be lower in these Angelman syndrome patients in conjunction with Ube3a deficiency.

Here, we have shown that the GABAergic dysfunction in Ube3a deficiency is caused by attenuated degradation of GAT1. The ubiquitin-proteasome degradation pathway has been recently implicated as a key regulator of neuronal activity by controlling the membrane trafficking and stability of receptor channels (*53*, *54*) and transporters (*55*). To the best of our knowledge, a specific E3 ligase and its target proteins have not been determined in inhibitory systems. Given that GAT1 and Ube3a expression increases during neurodevelopment (*56*, *57*), this study provides new insight into the synaptic plasticity of inhibitory neural systems and their pathophysiological contribution to neurodevelopmental disorders.

MATERIALS AND METHODS

Animals

All experiments conformed to the guidelines for the ethical use of animals for experimentation issued by Hamamatsu University School of Medicine. *Ube3a*-null mutant mice were generated on a C57BL/6 genetic background at Nagasaki University (*8*) and shipped to Hamamatsu University School of Medicine for all experimental procedures. A heterogeneous female mouse lacking a paternal *Ube3a* gene was crossed with a wild-type male mouse to obtain either heterogeneous mice lacking the maternal *Ube3a* gene (*Ube3a*$^{m-/p+}$) or littermate wild-type mice. Genotyping was carried out by polymerase chain reaction (PCR) of mouse tail DNA as described previously (*8*).

Electrophysiology

Unless otherwise noted, we carried out all electrophysiological analyses in P25 to P28 *Ube3a*$^{m-/p+}$ or littermate wild-type mice. Recordings from mice of each genotype were performed on consecutive days whenever possible. Recording temperature was set at 35°C except for the initial series of recordings for tonic currents at P25 to P28 or P75 to P82, which were recorded at room temperature. We evaluated the tonic currents by focal application of BIC (20 μM). For the first series of experiments (Fig. 1A, C and D), we also evaluated the tonic current by application of SR95531 (10 μM). Because the results obtained using BIC and SR95531 were not different (fig. S10), consistent with the findings of a previous report (*58*), we pooled both groups of data for further analyses. Detailed protocols are available in Supplementary Materials and Methods.

Immunoblotting

Mouse (P28 to P33) cerebellum samples were homogenized and lysed in lysis buffer. Blots were probed with antibodies and detected using horseradish peroxidase–conjugated secondary antibody and an enhanced luminescence kit (GE Healthcare). The experimental details and a list of antibodies are provided in Supplementary Materials and Methods.

Real-time PCR

Total RNAs obtained from mouse (P28 to P33) cerebellar samples were extracted with TRIzol reagent (Invitrogen). Complementary DNAs (cDNAs) were synthesized and quantitative real-time PCR was performed to validate the expression changes of selected genes in accordance with the manufacturer's protocols. Real-time PCRs were carried out in triplicate for each sample. Details are shown in Supplementary Materials and Methods.

Analysis of the interaction between Ube3a and GAT1

HEK293 cells were maintained in Dulbecco's modified Eagle's medium supplemented with 10% fetal bovine serum. cDNAs encoding mouse GAT1 (*59*) (provided by H. A. Lester, California Institute of Technology) were cloned into pCMV-3Tag-8 (Invitrogen). The pcDNA3-Myc3-E6AP (Ube3a) expression plasmid was provided by T. Ohta (St. Marianna University School of Medicine). Plasmids were transfected into HEK293 cells with the calcium phosphate method. For immunoprecipitation, cell lysates were incubated with 2 μg of antibodies and protein G+ Sepharose 4FF (GE Healthcare) at 4°C for 1 hour as previously described (*26*). Immunocomplexes were washed five times with lysis buffer. Immunoprecipitated samples as well as the original cell lysates (input) were separated by 7% SDS-PAGE and transferred from the gel onto a polyvinylidene difluoride membrane (Millipore), followed by immunoblotting. Proteins were visualized with an enhanced chemiluminescence system (Perkin Elmer). Details of the methods of endogenous protein analysis are provided in Supplementary Materials and Methods.

In vitro degradation assay

Mouse (P28 to P33) cerebellum samples were extracted with lysis buffer as described above. Cerebellum lysate (100 μg) was incubated in 20 μl of ubiquitination mixture [50 mM tris-HCl (pH 8.3), 5 mM $MgCl_2$, 2 mM dithiothreitol, 5 mM adenosine 5′-triphosphate, and ubiquitin (1 mg/ml)] for 0, 1, 2, 4, or 8 hours at 37°C. After incubation, each sample was subjected to 8% SDS-PAGE, followed by immunoblot analysis with anti-GAT1 antibody (Abcam) or α-tubulin antibody (Sigma). Details can be found in previous reports (*60*).

In vivo analysis of motor functions

All in vivo analyses were performed with male or female mice aged 3 to 5 months. For the footprint analysis and the tail suspension test, evaluators were unaware of either the genotype or the injected drug until analyses were completed. Except for the footprint analysis, the effect of THIP was evaluated 30 to 45 min after intraperitoneal administration. For the footprint analysis, hind paws were painted with black ink. Mice were then allowed to walk in a narrow corridor placed on white paper. We averaged the measurements from three trials for each recording. For the tail suspension test, mice were suspended by the tail; after stabilization, the clasping reflex was evaluated according to previously described scoring scales (*38*). Upper limb angles against body axes were evaluated by photographic capture of limb positions from a lateral view. For accelerating rotarod analysis, the rotational speed increased from 5 to 50 rpm over a period of 5 min. Three trials were performed for each recording, and median values were used for statistical analyses. Details are provided in Supplementary Materials and Methods.

Statistical analyses

Unless otherwise noted, statistical analyses were performed with unpaired Student's *t* tests. ANOVA (one- or two-way) and Bonferroni post hoc analysis were used to analyze multiple comparisons. Two-group comparisons were made with Student's *t* tests, except for the cases of sIPSC frequency and Purkinje cell firing properties. These were analyzed with Mann-Whitney *U* tests. Data are presented as means ± SEM, and $P < 0.05$ was considered to represent statistical significance.

SUPPLEMENTARY MATERIALS

www.sciencetranslationalmedicine.org/cgi/content/full/4/163/163ra157/DC1
Materials and Methods
Fig. S1. Ubiquitous expression of maternally expressed Ube3a in the cerebellar cortex.
Fig. S2. Electron micrographs of the cerebellar granule layer in wild-type and *Ube3a*$^{m-/p+}$ mice.
Fig. S3. Unaltered sIPSCs of cerebellar granule cells from *Ube3a*$^{m-/p+}$ mice.
Fig. S4. Accumulation of GAT1 protein in 5-month-old *Ube3a*$^{m-/p+}$ mouse cerebellum.
Fig. S5. Effects of THIP on cerebellar granule cell membrane excitability in wild-type and *Ube3a*$^{m-/p+}$ mice.
Fig. S6. Effects of THIP on Purkinje cell firing patterns in wild-type mice.
Fig. S7. Firing properties of Purkinje cells that display tonic firing.
Fig. S8. Effects of THIP administration on motor functions in wild-type mice.
Fig. S9. Scoring for the clasping reflex during the tail suspension test.
Fig. S10. Comparison of tonic currents after treatments with BIC and SR95531.
Table S1. Resting membrane and firing properties of cerebellar granule cells from wild-type and *Ube3a*$^{m-/p+}$ mice.
Table S2. Primers for PCR.
Movie S1. Tail suspension test.

REFERENCES AND NOTES

1. U. Albrecht, J. S. Sutcliffe, B. M. Cattanach, C. V. Beechey, D. Armstrong, G. Eichele, A. L. Beaudet, Imprinted expression of the murine Angelman syndrome gene, *Ube3a*, in hippocampal and Purkinje neurons. *Nat. Genet.* **17**, 75–78 (1997).
2. Y. H. Jiang, D. Armstrong, U. Albrecht, C. M. Atkins, J. L. Noebels, G. Eichele, J. D. Sweatt, A. L. Beaudet, Mutation of the Angelman ubiquitin ligase in mice causes increased cytoplasmic p53 and deficits of contextual learning and long-term potentiation. *Neuron* **21**, 799–811 (1998).
3. T. Kishino, M. Lalande, J. Wagstaff, UBE3A/E6-AP mutations cause Angelman syndrome. *Nat. Genet.* **15**, 70–73 (1997).
4. C. A. Williams, H. Angelman, J. Clayton-Smith, D. J. Driscoll, J. E. Hendrickson, J. H. Knoll, R. E. Magenis, A. Schinzel, J. Wagstaff, E. M. Whidden, R. T. Zori, Angelman syndrome: Consensus for diagnostic criteria. Angelman Syndrome Foundation. *Am. J. Med. Genet.* **56**, 237–238 (1995).
5. E. J. Weeber, Y. H. Jiang, Y. Elgersma, A. W. Varga, Y. Carrasquillo, S. E. Brown, J. M. Christian, B. Mirnikjoo, A. Silva, A. L. Beaudet, J. D. Sweatt, Derangements of hippocampal calcium/calmodulin-dependent protein kinase II in a mouse model for Angelman mental retardation syndrome. *J. Neurosci.* **23**, 2634–2644 (2003).
6. K. Yashiro, T. T. Riday, K. H. Condon, A. C. Roberts, D. R. Bernardo, R. Prakash, R. J. Weinberg, M. D. Ehlers, B. D. Philpot, Ube3a is required for experience-dependent maturation of the neocortex. *Nat. Neurosci.* **12**, 777–783 (2009).
7. P. L. Greer, R. Hanayama, B. L. Bloodgood, A. R. Mardinly, D. M. Lipton, S. W. Flavell, T. K. Kim, E. C. Griffith, Z. Waldon, R. Maehr, H. L. Ploegh, S. Chowdhury, P. F. Worley, J. Steen, M. E. Greenberg, The Angelman Syndrome protein Ube3A regulates synapse development by ubiquitinating arc. *Cell* **140**, 704–716 (2010).
8. K. Miura, T. Kishino, E. Li, H. Webber, P. Dikkes, G. L. Holmes, J. Wagstaff, Neurobehavioral and electroencephalographic abnormalities in *Ube3a* maternal-deficient mice. *Neurobiol. Dis.* **9**, 149–159 (2002).
9. B. Dan, S. G. Boyd, Angelman syndrome reviewed from a neurophysiological perspective. The *UBE3A-GABRB3* hypothesis. *Neuropediatrics* **34**, 169–176 (2003).
10. J. J. Yi, M. D. Ehlers, Emerging roles for ubiquitin and protein degradation in neuronal function. *Pharmacol. Rev.* **59**, 14–39 (2007).
11. A. C. Lossie, M. M. Whitney, D. Amidon, H. J. Dong, P. Chen, D. Theriaque, A. Hutson, R. D. Nicholls, R. T. Zori, C. A. Williams, D. J. Driscoll, Distinct phenotypes distinguish the molecular classes of Angelman syndrome. *J. Med. Genet.* **38**, 834–845 (2001).
12. K. Egawa, N. Asahina, H. Shiraishi, K. Kamada, F. Takeuchi, S. Nakane, A. Sudo, S. Kohsaka, S. Saitoh, Aberrant somatosensory-evoked responses imply GABAergic dysfunction in Angelman syndrome. *Neuroimage* **39**, 593–599 (2008).
13. I. Mody, R. A. Pearce, Diversity of inhibitory neurotransmission through $GABA_A$ receptors. *Trends Neurosci.* **27**, 569–575 (2004).
14. M. Farrant, Z. Nusser, Variations on an inhibitory theme: Phasic and tonic activation of $GABA_A$ receptors. *Nat. Rev. Neurosci.* **6**, 215–229 (2005).
15. Z. Nusser, W. Sieghart, P. Somogyi, Segregation of different $GABA_A$ receptors to synaptic and extrasynaptic membranes of cerebellar granule cells. *J. Neurosci.* **18**, 1693–1703 (1998).
16. D. W. Cope, G. Di Giovanni, S. J. Fyson, G. Orbán, A. C. Errington, M. L. Lorincz, T. M. Gould, D. A. Carter, V. Crunelli, Enhanced tonic $GABA_A$ inhibition in typical absence epilepsy. *Nat. Med.* **15**, 1392–1398 (2009).
17. A. N. Clarkson, B. S. Huang, S. E. MacIsaac, I. Mody, S. T. Carmichael, Reducing excessive GABA-mediated tonic inhibition promotes functional recovery after stroke. *Nature* **468**, 305–309 (2010).
18. S. V. Dindot, B. A. Antalffy, M. B. Bhattacharjee, A. L. Beaudet, The Angelman syndrome ubiquitin ligase localizes to the synapse and nucleus, and maternal deficiency results in abnormal dendritic spine morphology. *Hum. Mol. Genet.* **17**, 111–118 (2008).
19. M. J. Wall, M. M. Usowicz, Development of action potential-dependent and independent spontaneous $GABA_A$ receptor-mediated currents in granule cells of postnatal rat cerebellum. *Eur. J. Neurosci.* **9**, 533–548 (1997).
20. D. J. Rossi, M. Hamann, Spillover-mediated transmission at inhibitory synapses promoted by high affinity α_6 subunit $GABA_A$ receptors and glomerular geometry. *Neuron* **20**, 783–795 (1998).
21. V. Santhakumar, H. J. Hanchar, M. Wallner, R. W. Olsen, T. S. Otis, Contributions of the $GABA_A$ receptor α6 subunit to phasic and tonic inhibition revealed by a naturally occurring polymorphism in the α6 gene. *J. Neurosci.* **26**, 3357–3364 (2006).
22. A. Gadea, A. M. López-Colomé, Glial transporters for glutamate, glycine, and GABA: II. GABA transporters. *J. Neurosci. Res.* **63**, 461–468 (2001).
23. C. S. Chiu, S. Brickley, K. Jensen, A. Southwell, S. McKinney, S. Cull-Candy, I. Mody, H. A. Lester, GABA transporter deficiency causes tremor, ataxia, nervousness, and increased GABA-induced tonic conductance in cerebellum. *J. Neurosci.* **25**, 3234–3245 (2005).
24. R. M. Gustin, T. J. Bichell, M. Bubser, J. Daily, I. Filonova, D. Mrelashvili, A. Y. Deutch, R. J. Colbran, E. J. Weeber, K. F. Haas, Tissue-specific variation of Ube3a protein expression in rodents and in a mouse model of Angelman syndrome. *Neurobiol. Dis.* **39**, 283–291 (2010).
25. A. Togawa, T. Yamamoto, H. Suzuki, H. Fukasawa, N. Ohashi, Y. Fujigaki, K. Kitagawa, T. Hattori, M. Kitagawa, A. Hishida, Ubiquitin-dependent degradation of Smad2 is increased in the glomeruli of rats with anti-thymocyte serum nephritis. *Am. J. Pathol.* **163**, 1645–1652 (2003).
26. H. Fukasawa, T. Yamamoto, Y. Fujigaki, T. Misaki, N. Ohashi, T. Takayama, S. Suzuki, S. Mugiya, T. Oda, C. Uchida, K. Kitagawa, T. Hattori, H. Hayashi, S. Ozono, M. Kitagawa, A. Hishida,

Reduction of transforming growth factor-β type II receptor is caused by the enhanced ubiquitin-dependent degradation in human renal cell carcinoma. *Int. J. Cancer* **127**, 1517–1525 (2010).
27. V. M. Korkhov, H. Farhan, M. Freissmuth, H. H. Sitte, Oligomerization of the γ-aminobutyric acid transporter-1 is driven by an interplay of polar and hydrophobic interactions in transmembrane helix II. *J. Biol. Chem.* **279**, 55728–55736 (2004).
28. H. Farhan, V. Reiterer, V. M. Korkhov, J. A. Schmid, M. Freissmuth, H. H. Sitte, Concentrative export from the endoplasmic reticulum of the γ-aminobutyric acid transporter 1 requires binding to SEC24D. *J. Biol. Chem.* **282**, 7679–7689 (2007).
29. S. G. Brickley, S. G. Cull-Candy, M. Farrant, Development of a tonic form of synaptic inhibition in rat cerebellar granule cells resulting from persistent activation of $GABA_A$ receptors. *J. Physiol.* **497** (Pt. 3), 753–759 (1996).
30. M. Hamann, D. J. Rossi, D. Attwell, Tonic and spillover inhibition of granule cells control information flow through cerebellar cortex. *Neuron* **33**, 625–633 (2002).
31. P. Chadderton, T. W. Margrie, M. Häusser, Integration of quanta in cerebellar granule cells during sensory processing. *Nature* **428**, 856–860 (2004).
32. S. G. Brickley, V. Revilla, S. G. Cull-Candy, W. Wisden, M. Farrant, Adaptive regulation of neuronal excitability by a voltage-independent potassium conductance. *Nature* **409**, 88–92 (2001).
33. N. Brown, J. Kerby, T. P. Bonnert, P. J. Whiting, K. A. Wafford, Pharmacological characterization of a novel cell line expressing human $\alpha_4\beta_3\delta$ $GABA_A$ receptors. *Br. J. Pharmacol.* **136**, 965–974 (2002).
34. M. Womack, K. Khodakhah, Active contribution of dendrites to the tonic and trimodal patterns of activity in cerebellar Purkinje neurons. *J. Neurosci.* **22**, 10603–10612 (2002).
35. M. Sausbier, H. Hu, C. Arntz, S. Feil, S. Kamm, H. Adelsberger, U. Sausbier, C. A. Sailer, R. Feil, F. Hofmann, M. Korth, M. J. Shipston, H. G. Knaus, D. P. Wolfer, C. M. Pedroarena, J. F. Storm, P. Ruth, Cerebellar ataxia and Purkinje cell dysfunction caused by Ca^{2+}-activated K^+ channel deficiency. *Proc. Natl. Acad. Sci. U.S.A.* **101**, 9474–9478 (2004).
36. D. H. Heck, Y. Zhao, S. Roy, M. S. LeDoux, L. T. Reiter, Analysis of cerebellar function in *Ube3a*-deficient mice reveals novel genotype-specific behaviors. *Hum. Mol. Genet.* **17**, 2181–2189 (2008).
37. S. A. Mulherkar, N. R. Jana, Loss of dopaminergic neurons and resulting behavioural deficits in mouse model of Angelman syndrome. *Neurobiol. Dis.* **40**, 586–592 (2010).
38. E. M. Aloy, O. Weinmann, C. Pot, H. Kasper, D. A. Dodd, T. Rülicke, F. Rossi, M. E. Schwab, Synaptic destabilization by neuronal Nogo-A. *Brain Cell Biol.* **35**, 137–156 (2006).
39. T. Cremers, B. Ebert, Plasma and CNS concentrations of Gaboxadol in rats following subcutaneous administration. *Eur. J. Pharmacol.* **562**, 47–52 (2007).
40. M. Kaneda, M. Farrant, S. G. Cull-Candy, Whole-cell and single-channel currents activated by GABA and glycine in granule cells of the rat cerebellum. *J. Physiol.* **485** (Pt. 2), 419–435 (1995).
41. S. De Biasi, L. Vitellaro-Zuccarello, N. C. Brecha, Immunoreactivity for the GABA transporter-1 and GABA transporter-3 is restricted to astrocytes in the rat thalamus. A light and electron-microscopic immunolocalization. *Neuroscience* **83**, 815–828 (1998).
42. C. Kuenzle, M. Steinlin, G. Wohlrab, E. Boltshauser, B. Schmitt, Adverse effects of vigabatrin in Angelman syndrome. *Epilepsia* **39**, 1213–1215 (1998).
43. J. Voss, C. Sanchez, S. Michelsen, B. Ebert, Rotarod studies in the rat of the $GABA_A$ receptor agonist gaboxadol: Lack of ethanol potentiation and benzodiazepine cross-tolerance. *Eur. J. Pharmacol.* **482**, 215–222 (2003).
44. M. B. Herd, N. Foister, D. Chandra, D. R. Peden, G. E. Homanics, V. J. Brown, D. J. K. Balfour, J. J. Lambert, D. Belelli, Inhibition of thalamic excitability by 4,5,6,7-tetrahydroisoxazolo [4,5-c]pyridine-3-ol: A selective role for δ-$GABA_A$ receptors. *Eur. J. Neurosci.* **29**, 1177–1187 (2009).
45. P. D. Suzdak, C. Foged, K. E. Andersen, Quantitative autoradiographic characterization of the binding of [^{3}H]tiagabine (NNC 05-328) to the GABA uptake carrier. *Brain Res.* **647**, 231–241 (1994).
46. A. Friemel, B. Ebert, P. H. Hutson, P. Brust, K. Nieber, W. Deuther-Conrad, Postnatal development and kinetics of [^{3}H]gaboxadol binding in rat brain: In vitro homogenate binding and quantitative autoradiography. *Brain Res.* **1170**, 39–47 (2007).
47. H. Kaphzan, S. A. Buffington, J. I. Jung, M. N. Rasband, E. Klann, Alterations in intrinsic membrane properties and the axon initial segment in a mouse model of Angelman syndrome. *J. Neurosci.* **31**, 17637–17648 (2011).
48. I. van Welie, S. du Lac, Bidirectional control of BK channel open probability by CAMKII and PKC in medial vestibular nucleus neurons. *J. Neurophysiol.* **105**, 1651–1659 (2011).
49. G. Cheron, L. Servais, J. Wagstaff, B. Dan, Fast cerebellar oscillation associated with ataxia in a mouse model of Angelman syndrome. *Neuroscience* **130**, 631–637 (2005).
50. N. Asahina, T. Shiga, K. Egawa, H. Shiraishi, S. Kohsaka, S. Saitoh, [^{11}C]Flumazenil positron emission tomography analyses of brain gamma-aminobutyric acid type A receptors in Angelman syndrome. *J. Pediatr.* **152**, 546–549 (2008).
51. W. H. Roden, L. D. Peugh, L. A. Jansen, Altered $GABA_A$ receptor subunit expression and pharmacology in human Angelman syndrome cortex. *Neurosci. Lett.* **483**, 167–172 (2010).
52. F. Crestani, R. Keist, J. M. Fritschy, D. Benke, K. Vogt, L. Prut, H. Blüthmann, H. Möhler, U. Rudolph, Trace fear conditioning involves hippocampal α_5 $GABA_A$ receptors. *Proc. Natl. Acad. Sci. U.S.A.* **99**, 8980–8985 (2002).
53. C. Altier, A. Garcia-Caballero, B. Simms, H. You, L. Chen, J. Walcher, H. W. Tedford, T. Hermosilla, G. W. Zamponi, The Cavβ subunit prevents RFP2-mediated ubiquitination and proteasomal degradation of L-type channels. *Nat. Neurosci.* **14**, 173–180 (2011).
54. A. K. Fu, K. W. Hung, W. Y. Fu, C. Shen, Y. Chen, J. Xia, K. O. Lai, N. Y. Ip, APC^{Cdh1} mediates EphA4-dependent downregulation of AMPA receptors in homeostatic plasticity. *Nat. Neurosci.* **14**, 181–189 (2011).
55. C. Boehmer, G. Henke, R. Schniepp, M. Palmada, J. D. Rothstein, S. Bröer, F. Lang, Regulation of the glutamate transporter EAAT1 by the ubiquitin ligase Nedd4-2 and the serum and glucocorticoid-inducible kinase isoforms SGK1/3 and protein kinase B. *J. Neurochem.* **86**, 1181–1188 (2003).
56. C. Takayama, Y. Inoue, Developmental expression of GABA transporter-1 and 3 during formation of the GABAergic synapses in the mouse cerebellar cortex. *Brain Res. Dev. Brain Res.* **158**, 41–49 (2005).
57. M. Sato, M. P. Stryker, Genomic imprinting of experience-dependent cortical plasticity by the ubiquitin ligase gene *Ube3a*. *Proc. Natl. Acad. Sci. U.S.A.* **107**, 5611–5616 (2010).
58. P. I. Ortinski, J. R. Turner, A. Barberis, G. Motamedi, R. P. Yasuda, B. B. Wolfe, K. J. Kellar, S. Vicini, Deletion of the $GABA_A$ receptor α1 subunit increases tonic $GABA_A$ receptor current: A role for GABA uptake transporters. *J. Neurosci.* **26**, 9323–9331 (2006).
59. S. Mager, N. Kleinberger-Doron, G. I. Keshet, N. Davidson, B. I. Kanner, H. A. Lester, Ion binding and permeation at the GABA transporter GAT1. *J. Neurosci.* **16**, 5405–5414 (1996).
60. K. Kitagawa, Y. Hiramatsu, C. Uchida, T. Isobe, T. Hattori, T. Oda, K. Shibata, S. Nakamura, A. Kikuchi, M. Kitagawa, Fbw7 promotes ubiquitin-dependent degradation of c-Myb: Involvement of GSK3-mediated phosphorylation of Thr-572 in mouse c-Myb. *Oncogene* **28**, 2393–2405 (2009).
61. K. Inoue, S. Ueno, A. Fukuda, Interaction of neuron-specific K^+-Cl^- cotransporter, KCC2, with brain-type creatine kinase. *FEBS Lett.* **564**, 131–135 (2004).
62. C. Uchida, S. Miwa, K. Kitagawa, T. Hattori, T. Isobe, S. Otani, T. Oda, H. Sugimura, T. Kamijo, K. Ookawa, H. Yasuda, M. Kitagawa, Enhanced Mdm2 activity inhibits pRB function via ubiquitin-dependent degradation. *EMBO J.* **24**, 160–169 (2005).
63. T. Sato, A modified method for lead staining of thin sections. *J. Electron Microsc.* **17**, 158–159 (1968).

Acknowledgments: We thank H. A. Lester (California Institute of Technology) and T. Ohta (St. Marianna University School of Medicine) for providing the pcDNA3.1-mGAT1 and pcDNA3-Myc3-E6AP (Ube3a) expression plasmids, respectively. **Funding:** This work was supported by a Grant-in-Aid for Young Scientists (B) from the Japan Society for the Promotion of Science #23791166 (K.E.); Grants-in-Aid for Scientific Research on Priority Areas from the Ministry of Education, Culture, Sports, Science, and Technology, Japan, #21026013 and 23115506 (to A.F.); and Grants-in-Aid for Scientific Research from the Japan Society for the Promotion of Science #22390041 (to A.F.). **Author contributions:** K.E., M.K., S.S., and A.F. participated in the design and interpretation of the data. K.E. performed the electrophysiological experiments. K.E. and M.T. performed the behavioral experiments. K.I., K.K., and M.K. performed the immunohistochemical experiments. C.T. performed electron microscopy. T.K. generated the Ube3a knockout mouse line. K.E. and A.F. wrote the manuscript. **Competing interests:** The authors declare that they have no competing interests.

Submitted 20 July 2012
Accepted 14 November 2012
Published 5 December 2012
10.1126/scitranslmed.3004655

Citation: K. Egawa, K. Kitagawa, K. Inoue, M. Takayama, C. Takayama, S. Saitoh, T. Kishino, M. Kitagawa, A. Fukuda, Decreased tonic inhibition in cerebellar granule cells causes motor dysfunction in a mouse model of Angelman syndrome. *Sci. Transl. Med.* **4**, 163ra157 (2012).

CLINICAL REPORT

AMERICAN JOURNAL OF medical genetics PART A

Aberrant Methylation of H19-DMR Acquired After Implantation Was Dissimilar in Soma Versus Placenta of Patients With Beckwith–Wiedemann Syndrome

Ken Higashimoto,[1] Kazuhiko Nakabayashi,[2] Hitomi Yatsuki,[1] Hokuto Yoshinaga,[1] Kosuke Jozaki,[1] Junichiro Okada,[3] Yoriko Watanabe,[3] Aiko Aoki,[4] Arihiro Shiozaki,[4] Shigeru Saito,[4] Kayoko Koide,[1] Tsunehiro Mukai,[5] Kenichiro Hata,[2] and Hidenobu Soejima[1]*

[1]Division of Molecular Genetics & Epigenetics, Department of Biomolecular Sciences, Faculty of Medicine, Saga University, Saga, Japan

[2]Department of Maternal–Fetal Biology, National Research Institute for Child Health and Development, Setagaya, Tokyo, Japan

[3]Department of Pediatrics, Kurume University, Kurume, Japan

[4]Department of Obstetrics and Gynecology, University of Toyama, Toyama, Japan

[5]Nishikyushu University, Kanzaki, Saga, Japan

Manuscript Received: 7 October 2011; Manuscript Accepted: 19 January 2012

Gain of methylation (GOM) at the H19-differentially methylated region (H19-DMR) is one of several causative alterations in Beckwith–Wiedemann syndrome (BWS), an imprinting-related disorder. In most patients with epigenetic changes at H19-DMR, the timing of and mechanism mediating GOM is unknown. To clarify this, we analyzed methylation at the imprinting control regions of somatic tissues and the placenta from two unrelated, naturally conceived patients with sporadic BWS. Maternal H19-DMR was abnormally and variably hypermethylated in both patients, indicating epigenetic mosaicism. Aberrant methylation levels were consistently lower in placenta than in blood and skin. Mosaic and discordant methylation strongly suggested that aberrant hypermethylation occurred after implantation, when genome-wide de novo methylation normally occurs. We expect aberrant de novo hypermethylation of H19-DMR happens to a greater extent in embryos than in placentas, as this is normally the case for de novo methylation. In addition, of 16 primary imprinted DMRs analyzed, only H19-DMR was aberrantly methylated, except for NNAT DMR in the placental chorangioma of Patient 2. To our knowledge, these are the first data suggesting when GOM of H19-DMR occurs. © 2012 Wiley Periodicals, Inc.

Key words: Beckwith–Wiedemann syndrome; H19-DMR; aberrant DNA methylation; after implantation

How to Cite this Article:
Higashimoto K, Nakabayashi K, Yatsuki H, Yoshinaga H, Jozaki K, Okada J, Watanabe Y, Aoki A, Shiozaki A, Saito S, Koide K, Mukai T, Hata K, Soejima H. 2012. Aberrant methylation of H19-DMR acquired after implantation was dissimilar in soma versus placenta of patients with Beckwith–Wiedemann syndrome.
Am J Med Genet Part A 158A:1670–1675.

INTRODUCTION

Beckwith–Wiedemann syndrome (BWS) is an imprinting-related condition characterized by macrosomia, macroglossia, and abdominal wall defects (OMIM #130650). The relevant imprinted chromosomal region in BWS, 11p15.5, consists of two independent imprinted domains, *IGF2/H19* and *CDKN1C/KCNQ1OT1*. Imprinted genes within each domain are regulated by two imprinting control regions (ICR), the H19-differentially methylated region (H19-DMR) or KvDMR1 [Weksberg et al., 2010]. Several causative alterations have been identified in patients with BWS: loss of methylation (LOM) at KvDMR1, gain of methylation (GOM) at H19-DMR, paternal uniparental disomy (UPD), *CDKN1C* mutations, and chromosomal abnormality involving 11p15 [Sasaki et al., 2007; Weksberg et al., 2010].

Additional supporting information may be found in the online version of this article.

Grant sponsor: Japan Society for the Promotion of Science; Grant number: 20590330; Grant sponsor: Ministry of Health, Labor, and Welfare; Grant sponsor: National Center for Child Health and Development.

*Correspondence to:
Hidenobu Soejima, M.D., Ph.D., Professor, Division of Molecular Genetics & Epigenetics, Department of Biomolecular Sciences, Faculty of Medicine, Saga University, 5-1-1 Nabeshima, Saga 849-8501, Japan.
E-mail: soejimah@med.saga-u.ac.jp

Article first published online in Wiley Online Library (wileyonlinelibrary.com): 10 May 2012
DOI 10.1002/ajmg.a.35335

Methylation of H19-DMR is erased in primordial germ cells (PGCs) but becomes reestablished during spermatogenesis [Li, 2002; Sasaki and Matsui, 2008]: this methylation regulates the expression of *IGF2* and *H19* by functioning as a chromatin insulator, restricting access to shared enhancers [Bell and Felsenfeld, 2000; Hark et al., 2000]. GOM on the maternal H19-DMR leads to expression of both *IGF2* alleles and silencing of both *H19* alleles. Dominant maternal transmissions of microdeletions and/or base substitutions within H19-DMR have recently been reported in a few patients of BWS with H19-DMR GOM [Demars et al., 2010]. However, when and how the GOM on the maternal H19-DMR occurs is not clear.

Here, we found epigenetic mosaicism in two BWS patients. We also found that GOM at H19-DMR was discordant in blood and skin versus placenta; specifically, methylation levels were lower in placental samples. These findings strongly suggest that aberrant methylation of H19-DMR occurred after implantation. As a result, we expect aberrant de novo methylation happens to a greater extent in embryos than in placentas.

MATERIALS AND METHODS

Patients

Two unrelated patients with sporadic BWS, Patient 1 (BWS047) and Patient 2 (bwsh21-015), were delivered by cesarean in the third trimester of pregnancy. The mothers of both patients conceived naturally. Patient 1 and Patient 2 met clinical criteria for BWS as described by Elliott et al. [1994] and Weksberg et al. [2001], respectively (Table I). The placenta of Patient 1 was large and weighed 1,065 g, but was without any pathological abnormality. The placenta of Patient 2 was also large, weighing 1,620 g, and had an encapsulated placental chorangioma, as reported previously [Aoki et al., 2011]. The standard G-banding chromosome analysis using peripheral blood samples showed no abnormalities in either patient. This study was approved by the Ethics Committee for Human Genome and Gene Analyses of the Faculty of Medicine, Saga University.

Southern Blot Analysis

Genomic DNA was extracted from embryo-derived somatic tissues and the placentas of the patients (Fig. 1). Methylation-sensitive Southern blots with *Bam*HI and *Not*I were employed for KvDMR1, and blots with *Pst*I and *Mlu*I were employed for H19-DMR, as described previously [Soejima et al., 2004]. Band intensity was measured using the FLA-7000 fluoro-image analyzer (Fujifilm, Tokyo, Japan). The methylation index (MI, %) was then calculated (Fig. 1). Southern blots with *Apa*I were used to identify the microdeletion of H19-DMR as described previously [Sparago et al., 2004].

Bisulfite Sequencing and Combined Bisulfite Restriction Analysis (COBRA)

Bisulfite sequencing covering the sixth CTCF binding site (CTS6) was performed. For COBRA, PCR products of each primary imprinted DMR were digested with the appropriate restriction endonucleases and were then separated using the MultiNA Microchip Electrophoresis System (Shimazdu, Japan). The methylation index was also calculated. All PCR primer sets used in this study have been listed in Supplementary Table SI (See Supporting Information online).

DNA Polymorphism Analyses

For quantitative polymorphism analyses, tetranucleotide repeat markers (*D11S1997* and *HUMTH01*) and a triplet repeat marker (*D11S2362*) from 11p15.4–p15.5 were amplified and separated by electrophoresis on an Applied Biosystems 3130 genetic analyzer (Applied Biosystems, NY); data were quantitatively analyzed with the GeneMapper software. The peak height ratios of paternal allele to maternal allele were calculated. A single nucleotide polymorphism (SNP) for the *Rsa*I recognition site in *H19* exon 5 (rs2839703) was also quantitatively analyzed using hot-stop PCR [Uejima et al., 2000]. Band intensity was measured using the FLA-7000 fluoro-image analyzer (Fujifilm).

Mutation Search of H19-DMR

To search for mutations in the binding sites of CTCF, OCT4, and SOX2, we sequenced a genomic region in and around H19-DMR, which included seven CTCF-binding sites, three OCT4 sites, and one SOX2 site.

TABLE I. Clinical Information of BWS Patients

Patient ID	Conception	Birth weight (gestational age)	Clinical features	Karyotype	Placental weight and pathology	Placental–fetal weight ratio
Patient 1 (BWS047)	Natural	4,506 g (36w2d)	macrosomia macroglossia abdominal wall defect hypoglycemia	46,XY	1,065 g no pathological findings	0.236
Patient 2 (bwsh21-015)	Natural	2,540 g (33w5d)	macrosomia macroglossia hypoglycemia renal malformation hepatosplenomegaly	46,XX	1,620 g placental chorangioma	0.638

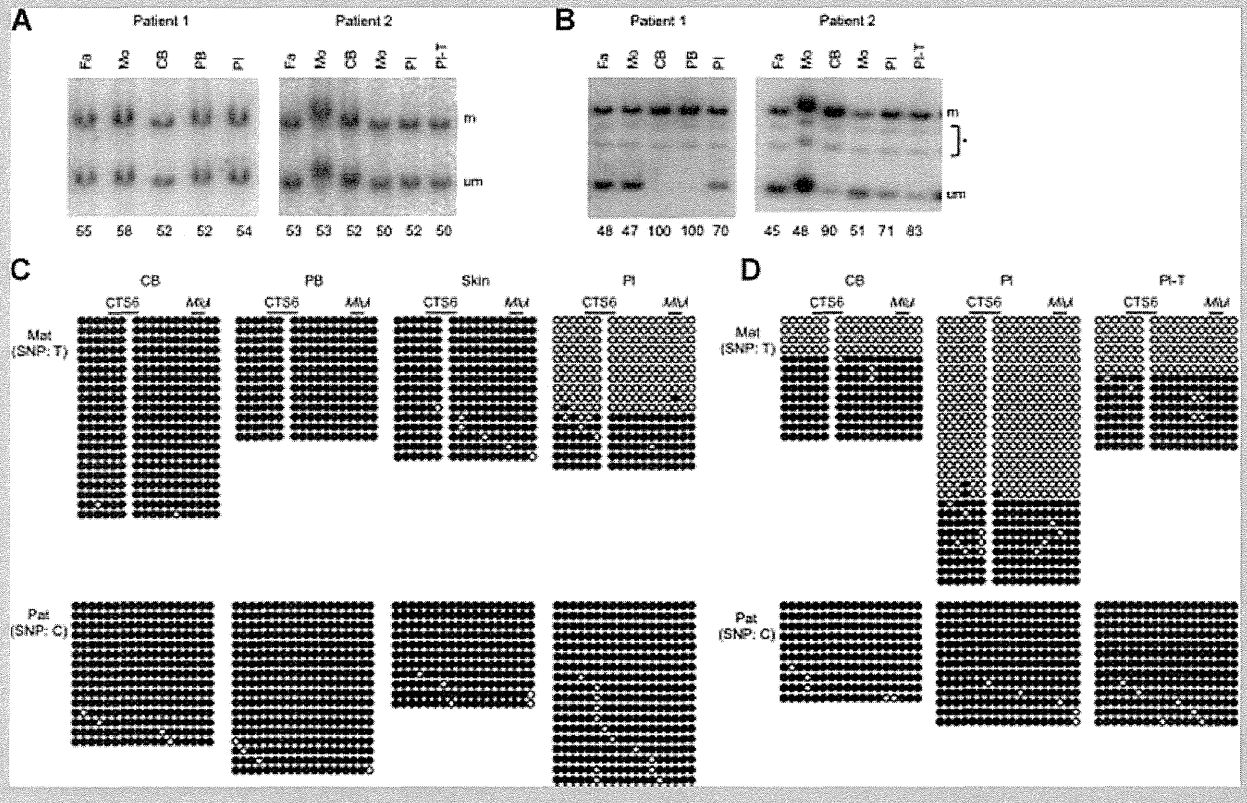

FIG. 1. Methylation analyses of KvDMR1 and H19-DMR. A: Methylation-sensitive Southern blots for KvDMR1. Genomic DNA was extracted from the cord blood, peripheral blood, skin, and placenta of Patient 1 and from the cord blood, placenta, and placental chorangioma of Patient 2. Methylation at KvDMR1 was normal in all samples analyzed. Methylation indices [MI, %] are shown under the figure. B: Methylation-sensitive Southern blots for H19-DMR. The MIs of blood samples were higher than the MIs of placental samples. MI was calculated using the equation $[M/(M+U)] \times 100$, where M is the intensity of the methylated band and U is the intensity of the unmethylated band. C: Bisulfite sequencing of H19-DMR in Patient 1. The two parental alleles were distinguishable by differences in SNPs. Both parental alleles were completely methylated in the cord blood, peripheral blood, and skin samples, and the maternal allele, which is normally unmethylated, was partially methylated in the placenta. D: Bisulfite sequencing of H19-DMR in Patient 2. Methylation of the maternal allele was higher in the cord blood than in the placenta or placental chorangioma. These results were consistent with the results of the Southern blot analysis. We confirmed complete methylation of paternal H19-DMR alleles and complete demethylation of maternal H19-DMR alleles in four normal control placentas that were heterozygous for identifiable SNPs (data not shown). Fa, father; Mo, mother; CB, cord blood; PB, peripheral blood; Pl, placenta; Pl-T, placental chorangioma; m, methylated band; um, unmethylated band; *, nonspecific bands; Mat, maternal allele; Pat, paternal allele; CTS6, sixth CTCF binding site; *MluI*, a restriction site approximately 80 bp downstream of CTS6 assayed by methylation-sensitive Southern blot and COBRA.

RESULTS

We first examined the methylation status of the two ICRs, KvDMR1, and H19-DMR, at 11p15.5 using methylation-sensitive Southern blot analysis. Methylation at KvDMR1 was normal in all samples collected (Fig. 1A); however, methylation at H19-DMR was aberrant (Fig. 1B). In Patient 1, hypermethylation at H19-DMR was complete in cord blood and peripheral blood samples (MI = 100%), and hypermethylation in the placenta was partial (MI = 70%). In Patient 2, H19-DMR was partially hypermethylated in cord blood (MI = 90%) but less so in the placenta and placental chorangioma (MI = 71% and MI = 83%, respectively). For further investigation of differences in methylation between the patients' somatic tissues and placentas, the CTS6 site was subjected to bisulfite sequencing (Fig. 1C and D). We could distinguish the two parental alleles in each patient sample using informative SNPs (rs10732516 and rs2071094). The maternal allele, which is normally unmethylated, was completely methylated in the cord blood, peripheral blood, and skin from Patient 1. However, in placental samples from Patient 1, the maternal allele was only partially methylated: 36% of all CpGs analyzed were methylated. Similar results were observed in Patient 2: the maternal allele in the cord blood was 68% methylated; however, the maternal allele was only 31% and 55% methylated in the placenta and chorangioma samples, respectively. The paternal alleles, which are normally fully methylated, were fully methylated in all samples. These findings supported the results of the Southern blots. Furthermore, we could not find any microdeletions or mutations in or around H19-DMR,

including seven CTCF-binding sites, three OCT4 sites, and one SOX2 site, indicating that there was no genetic cause of the hypermethylation (Fig. 2A and data not shown).

Next, we analyzed polymorphic markers at 11p15.4–p15.5 to determine whether copy number abnormalities or paternal UPD might be involved in these BWS patients. Although smaller PCR products were more easily amplified, paternal–maternal allele ratios in blood samples were between 0.92 and 1.33, indicating that both parental alleles were equally represented in both patients (Fig. 2B). Therefore, we could rule out copy number abnormality and paternal UPD within the patients' blood. We also investigated maternal contamination in the placenta. *D11S1997* and *HUMTH01* for Patient 1 and the *Rsa*I polymorphism in *H19* (rs2839703) for Patient 2 were used for this investigation because the mothers were expected to be homozygous for such polymorphisms. Thus, we investigated contamination of our samples by assessing the homozygosity of the polymorphisms in the mothers. The paternal–maternal ratios in Patient 1 were 0.94 and 1.03, indicating an equal contribution of both parental alleles and suggesting no contamination (Fig. 2B). In Patient 2, the ratios were 0.77 and 0.78 in the placenta and chorangioma, respectively, suggesting a small amount of contamination (Fig. 2C). However, such contamination was too

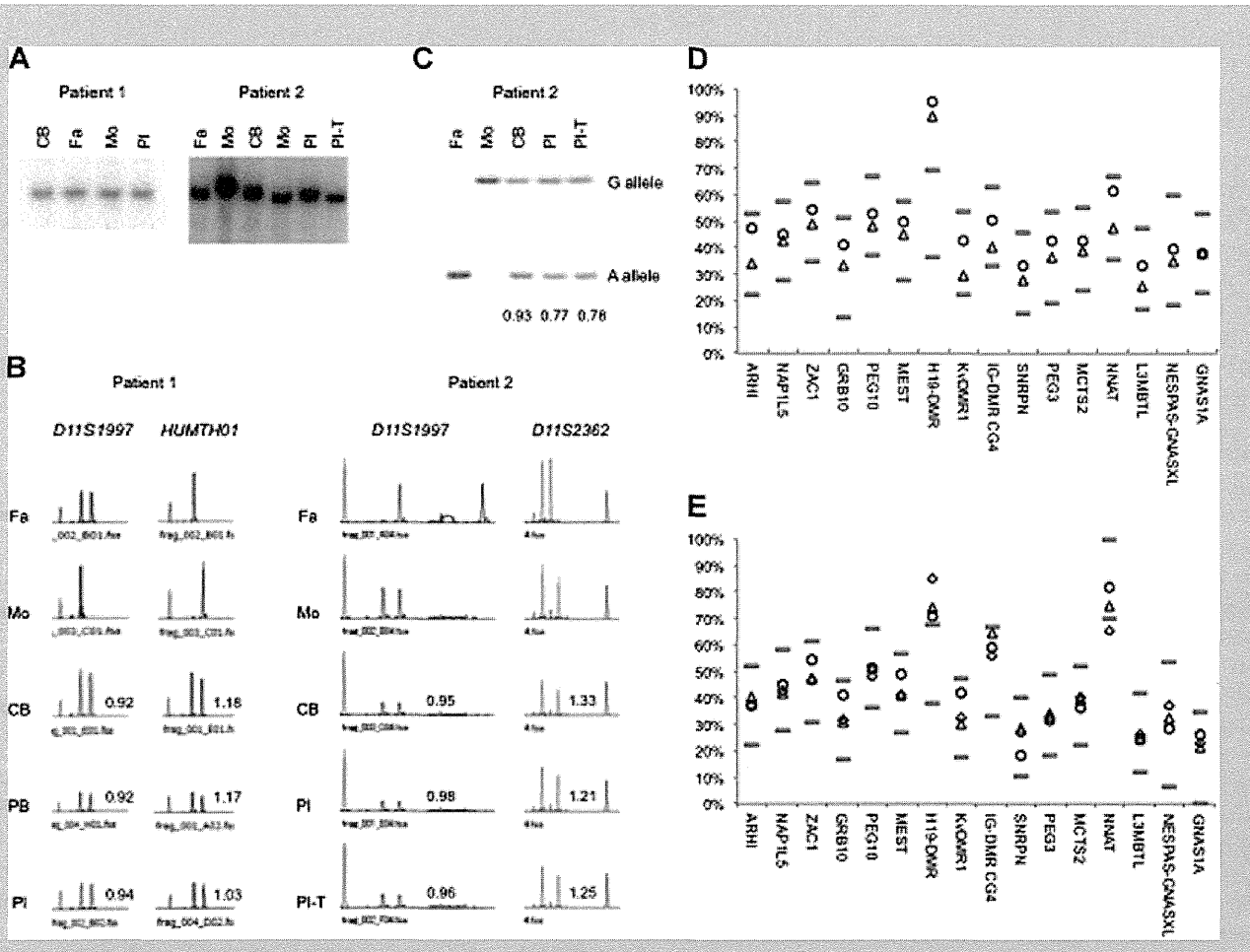

FIG. 2. Microdeletion analysis of H19-DMR, polymorphism analyses, and COBRA of primary imprinted DMRs in embryo-derived and placental samples. A: Southern blots identifying a microdeletion of H19-DMR. A genomic fragment (7.7 kb) generated by *Apa*I digestion, which included the entire H19-DMR, was evident in all samples, indicating that there was no microdeletion in this DMR. B: Microsatellite markers at 11p15.4–p15.5. The peak heights associated with each parental allele in all samples were quantitatively analyzed. The results indicated that both parental alleles were present and equally represented. C: Hot-stop PCR of an *Rsa*I polymorphic site in Patient 2. The ratios of paternal allele to maternal allele are shown under the figure. Although the ratios in the placenta and placental chorangioma are lower than in the cord blood, suggesting a small amount of maternal contamination, this was not enough to affect the results of the methylation analyses. COBRA of cord blood (D) and placentas (E), demonstrating that H19-DMR was hypermethylated. CTS6 is contained within H19-DMR. Methylation at other DMRs was normal in all samples, except for methylation at NNAT, which was aberrant in the placental chorangioma. Cord blood and placentas from 24 normal individuals were used as controls. The upper limit of normal methylation was defined as the higher of these two values: (1) the average of controls + 3 SD, or (2) the average + 15%. Similarly, the lower limit of normal methylation was definite as the lower of these two values: (1) the average of controls − 3 SD, or (2) the average − 15%. The upper and lower limits are indicated by gray bars. ○: Patient 1; △: Patient 2; ◇: placental chorangioma of Patient 2.

small to affect the results of the methylation analyses. In addition, sequence analysis did not show any mutations in *CDKN1C* (data not shown). These findings indicated that H19-DMR was aberrantly hypermethylated in both BWS patients and their associated placentas, but the aberrant methylation was consistently lower in the placenta, and that the H19-DMR GOM was strictly an isolated epimutation.

Finally, we analyzed the methylation status of 16 primary imprinted DMRs scattered throughout the genome-using COBRA (Fig. 2D and E). Only H19-DMR showed aberrant methylation among all primary DMRs in all samples, except for NNAT DMR, which was abnormal only in the placental chorangioma, indicating that the *IGF2/H19* imprinted domain was targeted for aberrant methylation in both somatic tissues and the placenta.

DISCUSSION

Methylation associated with parental imprints are erased in PGC and reestablished during gametogenesis in a sex-specific manner. The paternal pronucleus in the zygote undergoes active demethylation; extensive passive demethylation then ensues on maternal and paternal chromosomes during the pre-implantation period. After implantation, de novo methylation results in a rapid increase in DNA methylation in the inner cell mass (ICM), which gives rise to the entire embryo; in contrast, de novo methylation is either inhibited or not maintained in the trophoblast, which gives rise to the placenta [Li, 2002; Sasaki and Matsui, 2008]. The imprinted DMRs, however, escape these demethylation and de novo methylation events that occur in early embryogenesis. H19-DMR GOM in BWS patients is considered an error in imprint erasure in female PGCs [Horsthemke, 2010]. However, H19-DMR GOM, whether with or without microdeletions within H19-DMR, was partial, indicating a mosaic of normal cells and aberrantly methylated cells [Sparago et al., 2007; Cerrato et al., 2008]. These findings demonstrated that aberrant hypermethylation at H19-DMR was acquired after fertilization, although the precise timing was unknown.

Both participants in this study had isolated GOM at H19-DMR. The partial and variable hypermethylation among samples suggested epigenetic mosaicism. Furthermore, methylation levels in the placentas were lower than those in the blood and skin, suggesting that the aberrant methylation was acquired after implantation—when genome-wide de novo methylation normally occurs. Aberrant de novo methylation at H19-DMR is expected to be more widespread in the embryo than in the placenta, as this is normally the case for de novo methylation [Li, 2002; Sasaki and Matsui, 2008]; this disparity in efficiency could lead to the discordance between hypermethylation in trophoblast-derived placenta and that in embryo-derived blood and skin. This hypothesis is supported by a mouse experiment in which a mutant maternal allele harboring a deletion of four CTCF binding sites was hypomethylated in oocytes and blastocysts, yet was highly methylated after implantation [Engel et al., 2006]. To our knowledge, this is the first evidence demonstrating that aberrant hypermethylation of maternal H19-DMR is acquired after implantation in humans.

We found that of 16 primary imprinted DMRs analyzed, only H19-DMR showed aberrant methylation; even methylation at IG-DMR CG4, another paternally methylated, primary imprinted DMR, was normal in our patients. Although we only studied two patients, this finding indicated that the *IGF2/H19* imprinted domain in both the embryo and placenta was more susceptible than other imprinted domains to aberrant methylation acquired after implantation.

In conclusion, we found that methylation of H19-DMR was discordant in embryo-derived somatic tissue and placenta, strongly suggesting that the aberrant de novo methylation occurred after implantation. However, the precise mechanism of isolated H19-DMR GOM is still unknown. Since no mutations in *CTCF*, an important trans-acting imprinting factor, were found in these patients with isolated GOM at H19-DMR, the potential for mutations in the OCT and SOX transcription factors should be investigated because mutations of OCT-binding sites have previously been found in a few patients with H19-DMR GOM [Cerrato et al., 2008; Demars et al., 2010].

ACKNOWLEDGMENTS

This study was supported, in part, by a Grant-in-Aid for Scientific Research (C) (No. 20590330) from the Japan Society for the Promotion of Science, a Grant for Research on Intractable Diseases from the Ministry of Health, Labor, and Welfare, and a Grant for Child Health and Development from the National Center for Child Health and Development.

REFERENCES

Aoki A, Shiozaki A, Sameshima A, Higashimoto K, Soejima H, Saito S. 2011. Beckwith–Wiedemann syndrome with placental chorangioma due to H19-differentially methylated region hypermethylation: A case report. J Obstet Gynaecol Res 37:1872–1876.

Bell AC, Felsenfeld G. 2000. Methylation of a CTCF-dependent boundary controls imprinted expression of the Igf2 gene. Nature 405:482–485.

Cerrato F, Sparago A, Verde G, De Crescenzo A, Citro V, Cubellis MV, Rinaldi MM, Boccuto L, Neri G, Magnani C, D'Angelo P, Collini P, Perotti D, Sebastio G, Maher ER, Riccio A. 2008. Different mechanisms cause imprinting defects at the IGF2/H19 locus in Beckwith–Wiedemann syndrome and Wilms' tumour. Hum Mol Genet 17:1427–1435.

Demars J, Shmela ME, Rossignol S, Okabe J, Netchine I, Azzi S, Cabrol S, Le Caignec C, David A, Le Bouc Y, El-Osta A, Gicquel C. 2010. Analysis of the IGF2/H19 imprinting control region uncovers new genetic defects, including mutations of OCT-binding sequences, in patients with 11p15 fetal growth disorders. Hum Mol Genet 19:803–814.

Elliott M, Bayly R, Cole T, Temple IK, Maher ER. 1994. Clinical features and natural history of Beckwith–Wiedemann syndrome: Presentation of 74 new cases. Clin Genet 46:168–174.

Engel N, Thorvaldsen JL, Bartolomei MS. 2006. CTCF binding sites promote transcription initiation and prevent DNA methylation on the maternal allele at the imprinted H19/Igf2 locus. Hum Mol Genet 15:2945–2954.

Hark AT, Schoenherr CJ, Katz DJ, Ingram RS, Levorse JM, Tilghman SM. 2000. CTCF mediates methylation-sensitive enhancer-blocking activity at the H19/Igf2 locus. Nature 405:486–489.

Horsthemke B. 2010. Mechanisms of imprint dysregulation. Am J Med Genet C Semin Med Genet 154C:321–328.

Li E. 2002. Chromatin modification and epigenetic reprogramming in mammalian development. Nat Rev Genet 3:662–673.

Sasaki H, Matsui Y. 2008. Epigenetic events in mammalian germ-cell development: Reprogramming and beyond. Nat Rev Genet 9:129–140.

Sasaki K, Soejima H, Higashimoto K, Yatsuki H, Ohashi H, Yakabe S, Joh K, Niikawa N, Mukai T. 2007. Japanese and North American/European patients with Beckwith–Wiedemann syndrome have different frequencies of some epigenetic and genetic alterations. Eur J Hum Genet 15: 1205–1210.

Soejima H, Nakagawachi T, Zhao W, Higashimoto K, Urano T, Matsukura S, Kitajima Y, Takeuchi M, Nakayama M, Oshimura M, Miyazaki K, Joh K, Mukai T. 2004. Silencing of imprinted CDKN1C gene expression is associated with loss of CpG and histone H3 lysine 9 methylation at DMR-LIT1 in esophageal cancer. Oncogene 23:4380–4388.

Sparago A, Cerrato F, Vernucci M, Ferrero GB, Silengo MC, Riccio A. 2004. Microdeletions in the human H19 DMR result in loss of IGF2 imprinting and Beckwith–Wiedemann syndrome. Nat Genet 36:958–960.

Sparago A, Russo S, Cerrato F, Ferraiuolo S, Castorina P, Selicorni A, Schwienbacher C, Negrini M, Ferrero GB, Silengo MC, Anichini C, Larizza L, Riccio A. 2007. Mechanisms causing imprinting defects in familial Beckwith–Wiedemann syndrome with Wilms' tumour. Hum Mol Genet 16:254–264.

Uejima H, Lee MP, Cui H, Feinberg AP. 2000. Hot-stop PCR: A simple and general assay for linear quantitation of allele ratios. Nat Genet 25: 375–376.

Weksberg R, Nishikawa J, Caluseriu O, Fei YL, Shuman C, Wei C, Steele L, Cameron J, Smith A, Ambus I, Li M, Ray PN, Sadowski P, Squire J. 2001. Tumor development in the Beckwith–Wiedemann syndrome is associated with a variety of constitutional molecular 11p15 alterations including imprinting defects of KCNQ1OT1. Hum Mol Genet 10:2989–3000.

Weksberg R, Shuman C, Beckwith JB. 2010. Beckwith–Wiedemann syndrome. Eur J Hum Genet 18:8–14.

Human Reproduction, Vol.27, No.8 pp. 2541–2548, 2012
Advanced Access publication on June 6, 2012 doi:10.1093/humrep/des197

human reproduction ORIGINAL ARTICLE *Reproductive genetics*

Characterization of DNA methylation errors in patients with imprinting disorders conceived by assisted reproduction technologies

Hitoshi Hiura[1], Hiroaki Okae[1], Naoko Miyauchi[1], Fumi Sato[1], Akiko Sato[1], Mathew Van De Pette[2], Rosalind M John[2], Masayo Kagami[3], Kunihiko Nakai[4], Hidenobu Soejima[5], Tsutomu Ogata[6], and Takahiro Arima[1,*]

[1]Department of Informative Genetics, Environment and Genome Research Center, Tohoku University Graduate School of Medicine, 2-1 Seiryo-cho, Aoba-ku, Sendai 980-8575, Japan [2]Cardiff School of Biosciences, Museum Avenue, Cardiff CF10 3US, UK [3]Division of Clinical Genetics and Molecular Medicine, National Center for Child Health and Development, 2-10-1 Okura, Seatagaya-ku, Tokyo 157-8535, Japan [4]Department of Development and Environmental Medicine, Tohoku University Graduate School of Medicine, Sendai 980-8575, Japan [5]Division of Molecular Genetics and Epigenetics, Department of Biomolecular Sciences, Faculty of Medicine, Saga University, Saga 849-8501, Japan [6]Department of Pediatrics, Faculty of Medicine, Hamamatsu University, Hamamatsu 431-3192, Japan

*Correspondence address. Tel: +81-22-717-7844; Fax: +81 22-717-7063; E-mail: tarima@med.tohoku.ac.jp

Submitted on February 9, 2012; resubmitted on March 29, 2012; accepted on May 1, 2012

BACKGROUND: There is an increased incidence of rare imprinting disorders associated with assisted reproduction technologies (ARTs). The identification of epigenetic changes at imprinted loci in ART infants has led to the suggestion that the techniques themselves may predispose embryos to acquire imprinting errors and diseases. However, it is still unknown at what point(s) these imprinting errors arise, or the risk factors.

METHODS: In 2009 we conducted a Japanese nationwide epidemiological study of four well-known imprinting diseases to determine any association with ART. Using bisulfite sequencing, we examine the DNA methylation status of 22 gametic differentially methylated regions (gDMRs) located within the known imprinted loci in patients with Beckwith-Wiedemann syndrome (BWS, $n = 1$) and also Silver-Russell syndrome (SRS, $n = 5$) born after ART, and compared these with patients conceived naturally.

RESULTS: We found a 10-fold increased frequency of BWS and SRS associated with ART. The majority of ART cases showed aberrant DNA methylation patterns at multiple imprinted loci both maternal and paternal gDMRs (5/6), with both hyper- and hypomethylation events (5/6) and also mosaic methylation errors (5/6). Although our study may have been limited by a small sample number, the fact that many of the changes were mosaic suggested that they occurred after fertilization. In contrast, few of the patients who were conceived naturally exhibited a similar pattern of mosaic alterations. The differences in methylation patterns between the patients who were conceived naturally or after ART did not manifest due to the differences in the disease phenotypes in these imprinting disorders.

CONCLUSION: A possible association between ART and BWS/SRS was found, and we observed a more widespread disruption of genomic imprints after ART. The increased frequency of imprinting disorders after ART is perhaps not surprising given the major epigenetic events that take place during early development at a time when the epigenome is most vulnerable.

Key words: assisted reproduction technologies / genomic imprinting / DNA methylation / gametic differentially methylated regions / genomic imprinting disorders

Introduction

Human assisted reproduction technologies (ARTs) are used in the treatment of infertility and involve the manipulation of eggs and/or sperm in the laboratory. Several recent studies have identified an increased incidence of some normally very rare imprinting disorders after ART, including Beckwith-Wiedemann syndrome (BWS: ONIM 130650), Angelman syndrome (AS: ONIM 105830) and Silver-Russell syndrome (SRS: OMIM 180860) but not Prader-Willi syndrome (PWS: OMIM 176270; DeBaun *et al.*, 2003; Gosden *et al.*, 2003; Svensson *et al.*, 2005). Additionally, there are several reports suggesting that epigenetic alterations (epimutations) at imprinted loci occur during the *in vitro* manipulation of the gametes, with both IVF and ICSI approaches implicated (Cox *et al.*, 2002; DeBaun *et al.*, 2003; Gicquel *et al.*, 2003; Maher *et al.*, 2003; Moll *et al.*, 2003; Orstavik *et al.*, 2003; Ludwig *et al.*, 2005; Rossignol *et al.*, 2006; Bowdin *et al.*, 2007; Kagami *et al.*, 2007). However, some studies do not support a link between ART and imprinting disorders (Lidegaard *et al.*, 2005; Doornbos *et al.*, 2007).

Epigenetic marks laid down in the male or female germ lines, and which are inherited by the embryos, establish the imprinted expression of a set of developmentally important genes (Surani, 1998). Because imprinted genes are regulated by these gametic epigenetic marks, and by further epigenetic modifications in the somatic cell, they are particularly vulnerable to environmentally induced mutation. One of the best studied epigenetic marks is DNA methylation. DNA methylation is established in either the maternal or paternal germline at discrete genomic loci. This methylation is preserved in the fertilized embryo to generate differentially methylated regions (DMRs) which then signal to nearby genes to establish domains of imprinted chromatin by mechanisms that are not fully understood (John and Lefebvre, 2011). These germline or gametic DMRs (gDMRs) can orchestrate the monoallelic expression of genes over megabases of DNA (Tomizawa *et al.*, 2011) and are reset with every reproductive cycle (Lucifero *et al.*, 2002; Obata and Kono, 2002).

The increased frequency of epimutation(s) at imprinted loci in ART infants has led to the suggestion that ART procedures may induce imprinting error(s). However, these studies are confounded because ART populations are, by their very nature, different from populations who were conceived without the use of ART, with a low fertility rate, an increased frequency of reproductive loss and usually of advanced age, all of which are associated with increased occurrence of fetal and neonatal abnormalities. Furthermore, it is difficult to determine the causality of imprinting errors in any specific abnormality reported after ART. Both IVF and ICSI appear to be associated with an increased relative risk of imprinting disorders (Savage *et al.*, 2011). These procedures are often undertaken for unexpected infertility and require ovarian stimulation, oocyte collection and *in vitro* culture before the embryos are implanted. It has been suggested that infertility and any resulting ovarian stimulation may predispose to epigenetic errors (Sato *et al.*, 2007). Animal studies suggest that *in vitro* embryo culture may be associated with epigenetic alterations. In particular, the large offspring syndrome in cattle undergoing ART is associated with the loss of maternal allele methylation at insulin-like growth factor 2 receptor (*IGF2R*) gDMR (Young *et al.*, 2001) and has phenotypic similarity to BWS. It is still unknown when these imprinting errors arise and what factors predispose to epigenetic changes. Previously, Chang *et al.* (2005) reported no phenotypic differences between BWS patients who were conceived after ART and naturally. However, Lim *et al.* (2009) reported that patients who were conceived after ART had a significantly lower frequency of exomphalos and higher risk of non-Wilms tumor neoplasia. Phenotypic differences between patients who were conceived after ART and naturally are largely unreported, while any changes to phenotype may be altered by the frequency and the degree of epimutations. Studies revealed that some patients with BWS born after ART presented with epimutations that were not restricted to the 11p15 region (Rossignol *et al.*, 2006; Bliek *et al.*, 2009; Lim *et al.*, 2009). Further analysis of abnormal methylation patterns in imprinting disorders may provide clues as to the cause of disease and identify the ART-related risk factor(s).

To address these questions in this study, we engaged in a nationwide epidemiological study of the Japanese population to determine the frequency of four imprinting disorders after natural conception and after ART. We then analyzed the DNA methylation status of 22 gDMRs in BWS and SRS patients conceived by the two routes. Finally, we compared the abnormal methylation patterns and the phenotypes reported for both sets of patients. As a result we found that both BWS and SRS were more frequent after ART and that ART patients exhibited a higher frequency of aberrant DNA methylation patterns at multiple loci with, in some cases, mosaic methylation errors.

Materials and Methods

Nationwide investigation of imprinting disorders

The protocol was established by the Research Committee on the Epidemiology of Intractable Diseases. The protocol consisted of a two-stage postal survey. The first-stage survey was used to estimate the number of individuals with any of the four imprinting diseases: BWS, SRS, PWS and AS. The second-stage survey was used to identify the clinico-epidemiological features of these syndromes.

In the first-stage survey, the pediatric departments of all hospitals were identified based on a listing of hospitals, as at 2008, supplied by the R&D Co. Ltd (Nagoya, Japan). Hospitals were classified into seven categories according to the type of institution and the number of hospital beds. The survey was mailed to a total of 3158 departments in October 2009 with letters of request for participation in recording these diseases. A simple questionnaire was used to ask about the number of patients with any of the four imprinting disorders. Diagnosis was determined by karyotype analyses, genetic analyses and clinical phenotypes by their clinical doctors. In December 2009, a second request was sent to departments that had not responded to the earlier deadline (at the end of November 2009). Following the first-stage survey, we sent acknowledgement letters to departments that had responded.

The second questionnaires were forwarded to the departments that had reported patients with the imprinting disorders on the first questionnaires. Detailed clinical information for the patients with these imprinting disorders was collected, including the age, gender, growth and development pattern, the methods of the diagnosis, the presence of infertility treatment and the methods of ART where applicable. Duplicate results were excluded using the information regarding the patient's age and gender where available. The study was approved by the Ethics Committee of Tohoku University School of Medicine.

Estimation of prevalence of imprinting disorders

The number of patients, who were diagnosed by genetic and cytogenetic testing and by clinical phenotypes, was obtained from data from the departments who responded to the first survey. The 95% confidence interval (CI) was calculated as previously described (Wakai *et al.*, 1997). The prevalence was determined, based on the population of Japan in 2009 (127 510 000) with data from the Statistics Bureau of the Ministry of Internal Affairs and Communications.

DNA preparation

Genomic DNA was obtained from blood or buccal mucosal cell samples from patients with one of the imprinting disorders using standard extraction methods (Kobayashi *et al.*, 2007). For control DNAs, DNA was prepared from the sperm and cord blood samples from unaffected individuals. The study was performed after obtaining patients or their parents' consent.

Bisulfite-treatment PCR including the SNPs

We first searched for single nucleotide polymorphisms (SNPs) within 22 previously reported human gDMRs (Kikyo *et al.*, 1997; Smith *et al.*, 2003; Kobayashi *et al.*, 2006, 2009; Wood *et al.*, 2007) using 20 control Japanese blood DNA samples. PCR primer sets were designed to span these SNPs (Supplementary data, Table SI) and human sperm DNA and blood DNA was used to confirm that these PCR assays detected the methylation status of the 22 DMRs. Paternal DMRs were shown to be fully methylated in sperm DNA, maternal DMRs were fully unmethylated and in blood DNA, both paternal and maternal DMRs showed ~50% methylation (Supplementary data, Fig. S1). The human gDMRs and the non-imprinted repetitive long interspersed nucleotide element (*LINE1*) and *Alu* repetitive sequences were examined by bisulfite sequencing using established protocols (Kobayashi *et al.*, 2007). Briefly, PCR products were purified and cloned into the pGEM-T vector (Promega, Madison, WI, USA). Individual clones were sequenced using M13 reverse primer and an automated ABI Prism 3130xl Genetic Analyzer (Applied Biosystems, Foster City, CA, USA). On average, 20 clones were sequenced for each sample.

Statistics

The frequency of the manifestation in patients who were conceived after ART was compared with that observed in patients conceived naturally using Fisher's exact test.

Results

Frequency of four imprinting disorders and their association with ART

We first investigated the nationwide frequency of four imprinting disorders (BWS, AS, PWS and SRS) in Japan in the year 2009. Of a total of 3158 departments contacted, 1602 responded to the first-stage survey questionnaire (50.7%). The total number of cases was calculated using a second-stage survey ensuring the exclusion of duplicates (Table I). Using this information, and taking into account the number of patients with suspect clinical signs but without a formal diagnosis, we identified 444 BWS patients (95% CI: 351–538), 949 AS patients (95% CI: 682–1217), 2070 PWS patients (95% CI: 1504–2636) and 326 SRS patients (95% CI: 235–416). From these figures (and using the 2009 population of Japan: 127 510 000) we estimated the prevalence of these syndromes to be 1 in 287 000, 1 in 134 000, 1 in 62 000 and 1 in 392 000, respectively, for BWS, AS, PWS and SRS. Further details are given in Supplementary data, Table SII and Supplementary data, Fig. S2.

Table I The 2009 frequency of four imprinting diseases in Japan in relation to use of assisted reproduction techniques (ART).

Imprinting disorders	Total estimated patient number (95% CI)	The total prevalence of the syndrome	The number of patients after ART/ total (%)
BWS	444 (351–538)	1 in 287 000	6/70 (8.6)
AS	949 (682–1217)	1 in 134 000	2/123 (1.6)
PWS	2070 (1504–2636)	1 in 62 000	4/261 (1.5)
SRS	326 (235–416)	1 in 392 000	4/42 (9.5)

Results of a nationwide epidemiological investigation of four imprinting disorders in Japan, under the governance of the Ministry of Health, Labor and Welfare of the Japanese government. Precise diagnosis was performed using fluorescence *in situ* hybridization and DNA methylation analyses. The type of ART, obtained from the questionnaires, was compared with the frequencies of these diseases and the epimutation rates. BWS, Beckwith-Wiedemann syndrome, AS, Angelman syndrome, PWS, Prader-Willi syndrome; SRS, Silver-Russell syndrome.

Between 1997 and 2008, the period during which the ART babies in this study were born, 0.64–0.98% of the total number of babies born in Japan were born as a result of IVF and ICSI. We ascertained the frequency of ART procedures in the cases of BWS, AS, PWS and SRS via the questionnaire sent to doctors (Table I, Supplementary data, Table SIII). The numbers of patients with PWS and AS we identified was low; however, the frequency of ART in these cases was not dissimilar to that expected, based on the population rate of ART use, with 2/123 (1.6%) cases of AS and 4/261 (1.5%) cases of PWS born after ART. In contrast, for BWS and SRS the frequency of ART was nearly 10-fold higher than anticipated with 6/70 (8.6%) BWS and 4/42 (9.5%) SRS patients born after ART.

After analyzing the second questionnaire, the blood or buccal mucosal cell samples were obtained from 15 individuals with BWS, 23 with SRS, 73 with AS and 29 with PWS. Using polymorphic bisulfite-PCR sequencing, we examined the methylation status of gDMRs within these samples at the imprinted regions implicated in these syndromes. For BWS we assayed *H19* and *KCNQ1OT1* (*LIT1*) gDMRs, for SRS we assayed the *H19* gDMR and for PWS and AS we assayed the *SNRPN* gDMR. For all patients (conceived naturally and with ART), the frequencies of DNA methylation errors (epimutations) corrected were 7/15 (46.7%) for BWS, 9/23 (39.1%) for SRS, 6/73 (8.2%) for AS and 2/29 (6.9%) for PWS. When looking at the ART cases exclusively, epimutation rates were 3/5 (BWS), 3/7 (SRS), 0/2 (AS) and 0/2 (PWS).

Abnormal methylation patterns in the ART and naturally conceived SRS patients with epimutations.

While hypomethylation of *H19* at chromosome 11 is known to be a frequent occurrence in SRS (Bliek *et al.*, 2006), various additional loci at chromosomes 7, 8, 15, 17 and 18 have been implicated as having a

role in this syndrome (OMIM 180860). We first identified SNPs in the previously reported 22 human DMRs using genomic DNA isolated from human sperm and blood from unaffected individuals, which could then be used in bisulfite-PCR methylation assays to assign methylation to the parental allele. We next collected a total of 15 SRS samples, including previously collected samples (ART: 2, naturally conceived: 4), which had DNA methylation errors at the paternal gDMR at *H19*. Five of these were born from ART and 10 were from natural conceptions. We analyzed and compared the DNA methylation status of the 3 other paternal gDMRs and the 19 maternal gDMRs (Supplementary data, Fig. S3, Table, Supplementary data, Table SIV). In four out of the five ART cases, DNA methylation errors were not restricted to the *H19* gDMR, and were present at both maternally and paternally methylated gDMRs. These four cases showed a mixture of hyper- and hypomethylation with mosaic (partial) patterns. In contrast, only 3 of the 10 naturally conceived patients showed DNA methylation errors at loci other than *H19* gDMR.

To determine whether DNA methylation errors occurred in patients at a broader level in the genomes, we assessed the methylation profiles of the non-imprinted *LINE1* and *Alu* elements. We examined a total of 28 CpG sites in a 413-bp fragment of *LINE1* and 12 CpG sites in a 152-bp fragment of *Alu* (Supplementary data, Table SIV), and no significant differences were found in the methylation ratios between patients conceived by ART and naturally.

The abnormal methylation pattern in BWS patients with epimutations

In BWS, hypermethylation of *H19* or hypomethylation of *KCNQ1OT1(LIT1)* at human chromosome 11 are both frequently reported (Choufani *et al.*, 2010). We collected seven BWS samples with DNA methylation errors of the *LIT1* gDMR, one of which was derived from ART patient and six from naturally conceived patients (Supplementary data, Fig. S3, Table II, Supplementary data, Table SIV). In the one ART (ICSI) case, we identified four additionally gDMR methylation errors, again present at both maternally and paternally methylated gDMRs and with mixed hyper- and hypomethylation patterns. Furthermore, the methylation error at the *NESPAS* DMR was mosaic in this patient. One of the six naturally BWS cases had similar changes. Although we had only one BWS case conceived by ART, widespread methylation errors were similar to those for the DNA methylation error pattern in SRS.

Phenotypic differences between ART patients and those conceived naturally

The increased frequency of DNA methylation errors at other loci in the ART cases suggested that the BWS and SRS cases born after ART might exhibit additional phenotypic characteristics. However, when we compared in detail the clinical features from both categories of conception (Supplementary data, Table SV), we found no major differences between ART and naturally conceived patients with BWS and SRS.

Discussion

Our key finding from this study was a possible association between ART and the imprinting disorders, BWS and SRS. We did not find a similar association with PWS and AS but our numbers were quite low in this study and a larger due to the questionnaire return rate and relative rarity of the diseases, international study will be required to reach definitive conclusions. Furthermore, factors such as PCR and/or cloning bias in the bisulfite method and correction for changing rate of ART over time must be considered when analyzing any results.

In addition to the possible association between ART and BWS/SRS, we observed a more widespread disruption of genomic imprints after ART. The increased frequency of imprinting disorders after ART shown by us and others is perhaps not surprising given the major epigenetic events that take place during early development at a time when the epigenome is most vulnerable. The process of ART exposes the developing epigenome to many external influences, which have been shown to influence the proper establishment and maintenance of genomic imprints, including hormone stimulation (Sato *et al.*, 2007), *in vitro* culturing (DeBaun *et al.*, 2003; Gicquel *et al.*, 2003; Maher *et al.*, 2003), cryopreservation (Emiliani *et al.*, 2000; Honda *et al.*, 2001) and the timing of embryo transfer (Shimizu *et al.*, 2004; Miura and Niikawa, 2005). Furthermore, we and others have also shown that some infertile males, particularly those with oligozoospermia, carry pre-existing imprinting errors in their sperm (Marques *et al.*, 2004; Kobayashi *et al.*, 2007; Marques *et al.*, 2008) which might account for the association between ART and imprinting disorders.

Imprinting syndromes and their association with ART

We report the first Japanese nationwide epidemiological study to examine four well-known imprinting diseases and their possible association with ART. We found that the frequency of ART use in both BWS and SRS was higher than anticipated based on the nationwide frequency of ART use at the time when these patients were born. Several other reports have raised concerns that children conceived by ART have an increased risk of disorders (Cox *et al.*, 2002; DeBaun *et al.*, 2003; Maher *et al.*, 2003; Orstavik *et al.*, 2003; Ludwig *et al.*, 2005; Lim and Maher, 2009). However, the association is not clear in every study (Lidegaard *et al.*, 2005; Doornbos *et al.*, 2007). The studies reporting an association were mainly from case reports or case series whereas the studies where no association was reported were cohort studies. Therefore, the differences in the epidemiological analytical methods might accounts for the disparity in findings.

Owing to the rare nature of the imprinting syndromes, statistical analysis is challenging. In addition, the diagnosis of imprinting diseases is not always clear cut. Many of the syndromes have a broad clinical spectrum, different molecular pathogenesis, and the infant has to have reached a certain age before these diseases become clinically detectable. It is therefore likely that some children with these diseases are not recorded with the specific diagnosis code for these syndromes. Nonetheless, in this study we were examining the relationship between ART and the imprinting syndromes and these confounding factors are likely to apply equally to both groups.

Both BWS and SRS occurred after ART but our numbers for PWS and AS were low, precluding any definitive conclusion for these two disorders. However, while most cases of BWS and SRS are caused by an epimutation, epimutations are very rare in PWS and AS (only 1–4%) and ART would not be expected to increase chromosome 15

Table II Abnormal methylation in patients with SRS and BWS.

Case	ART	Abnormal methylation			
SRS					
SRS-1	IVF-ET	H19 hypomethylated (mosaic)	PEG1 hypermethylated	PEG10 hypermethylated (mosaic)	GRB10 hypermethylated; ZNF597 hypomethylated
SRS-2	IVF-ET	H19 hypomethylated (mosaic)			
SRS-3	IVF-ET	H19 hypomethylated (mosaic)	PEG1 hypermethylated (mosaic)		
SRS-4	IVF-ET	H19 hypomethylated	GRB10 hypermethylated		
SRS-5	IVF-ET	H19 hypomethylated (mosaic)	INPP5F hypermethylated		
SRS-6		H19 hypomethylated			
SRS-7		H19 hypomethylated (mosaic)	ZNF597 hypermethylated (mosaic)	ZNF331 hypomethylated (mosaic)	
SRS-8		H19 hypomethylated			
SRS-9		H19 hypomethylated (mosaic)			
SRS-10		H19 hypomethylated			
SRS-11		H19 hypomethylated (mosaic)	PEG1 hypermethylated		
SRS-12		H19 hypomethylated			
SRS-13		H19 hypomethylated (mosaic)	FAM50B hypomethylated		
SRS-14		H19 hypomethylated			
SRS-15		H19 hypomethylated			
BWS					
BWS-1	ICSI	LIT1 hypomethylated	ZDBF2 hypermethylated	PEG1 hypermethylated	NESPAS hypomethylated (mosaic)
BWS-2		LIT1 hypomethylated			
BWS-3		LIT1 hypomethylated			
BWS-4		LIT1 hypomethylated			
BWS-5		LIT1 hypomethylated			
BWS-6		LIT1 hypomethylated	ZDBF2 hypomethylated	ZNF331 hypomethylated (mosaic)	
BWS-7		LIT1 hypomethylated			

ET, embryo transfer. Summary of the abnormal methylation patterns in the ART conceived and naturally conceived patients with Silver-Russell syndrome (SRS) and Beckwith-Wiedemann syndrome (BWS) with epimutations. Numbers in parentheses show the results of the methylation rates obtained using bisulfite-PCR sequencing. The % of DNA methylation of 22 gDMRs in all patients with SRS and BWS examined are presented in Supplementary data, Table SIV. Depictions in red represent DMRs normally exclusively methylated on the maternal allele, while blue represent paternally methylated sites.

deletions or uniparental disomy, consistent with our findings. Prior to this investigation, there was some evidence for an increased prevalence of BWS after ART but less evidence for an increased prevalence of SRS, with five SRS patients reported linked to ART (Svensson *et al.*, 2005; Bliek *et al.*, 2006; Kagami *et al.*, 2007; Galli-Tsinopoulou *et al.*, 2008). Our population-wide study provides evidence to suggest that both BWS and SRS occur more frequently after ART in the Japanese population.

Mechanisms of epimutation in the patients conceived by ART

By performing a comprehensive survey of all the known gDMRs in a number of patients with BWS and SRS, we found that multiple loci were more likely to be affected in ART cases than those conceived naturally. Lim *et al.* (2009) have reported a similarly increased frequency of multiple errors after ART, with 37.5% of patients conceived with ART and 6.4% of naturally conceived patients displaying abnormal methylation at additional imprinted loci. However, while Bliek *et al.* (2009) reported alterations in multiple imprinted loci in 17 patients out of 81 BWS cases with hypomethylation of *KCNQ1OT1*(*LIT1*) ICR, only 1 of the cases with multiple alterations was born after ART. Similarly, Rossignol *et al.* (2006) reported that 3 of 11 (27%) ART-conceived patients and 7 of 29 (24%) naturally conceived patients displayed abnormal methylation at additional loci. In these four earlier studies, not all gDMRs were assayed and it may be that by doing so, these incongruities will be resolved.

The pattern of cellular mosaicism we observed in some patients suggested that the imprinting defects occurred after fertilization rather than in the gamete as DNA methylation alterations arising in the gamete would be anticipated to be present in every somatic cell. This suggested the possibility that the DNA methylation errors occurred as a consequence of impaired maintenance of the germline imprints rather than a failure to establish these imprints in the germline or a loss of these imprints in the sperm or oocytes *in vitro*. Furthermore, some patients conceived by ART with SRS and BWS showed

alterations at both maternally and paternally methylated gDMRs suggesting that the defects were not limited to one parental germline. The mechanisms controlling the protection of imprinted loci against demethylation early in the development remain unclear. Our data suggested that this protection may fail in ART resulting in the tissue-specific loss of imprints, though it remains unclear if this ever occurs naturally. Potential factors involved could include the culture conditions for the newly fertilized oocyte and the length of exposure to specific media or growth factors, as part of the ART procedure. Some of the naturally conceived patients also had abnormal methylation at both maternally and paternally methylated gDMRs, which were in some cases mosaic. This could indicate that fertility issues arise as a consequence of pre-existing mutations in factors required to protect and maintain imprints early in life and it may therefore be possible to identify genetic mutations in these factors in this group of patients.

Clinical features

In our large-scale epidemiological study, we found differences in the frequency of some classic features of SRS and BWS between patients conceived by ART and those conceived naturally. We found that 7/7 (100%) ART conceived SRS patients showed body asymmetry, whereas only 30/54 (55.5%) who were conceived naturally possessed this feature. Similarly in BWS, earlobe creases were present in 4/7 (57.1%) ART conceived cases and 44/89 (49.4%) naturally conceived, bulging eyes in 3/7 (42.8%) versus 21/89 (23.6%), exomphalos in 6/7 (85.7%) versus 61/89 (68.5%) and nephromegaly in 2/7 (28.6%) versus 18/89 (20.2%), respectively. It is therefore possible that the dysregulation of the additional genes does modify the typical SRS and BWS phenotypes (Azzi *et al.*, 2010). BWS patients with multiple hypermethylation sites have been reported with complex clinical phenotypes (Bliek *et al.*, 2009) and a recently recognized BWS-like syndrome involving overgrowth with severe developmental delay was reported after IVF/ICSI (Shah *et al.*, 2006).

In our study patients with diagnosed imprinting disorders that presented with defects at additional loci (i.e. other than the domain responsible for that disorder) did not display additional phenotypes not normally reported in BWS or SRS. Since we were effectively selecting for classic cases of BWS and SRS in the first instance, it is possible that there are individuals born through ART showing entirely novel or confounding phenotypes that were not identified in our survey. Alternatively, as many of the alterations we observed showed a mosaic pattern, it is possible that mosaic individuals have more subtle phenotypes. In light of this new information on mosaicism, we may be able to use our knowledge of the individual's epigenotype to uncover these subtle changes.

This study, and the work of our colleagues, highlights the pressing need to conduct long-term international studies on ART treatment and the prevalence of imprinting disorders, particularly as the use of ART is increasing worldwide. It remains to be seen if other very rare epigenetic disorders will also have a possible association with the use of ART. Furthermore, it is not yet known what other pathologies might be influenced by ART. For example, in addition to general growth abnormalities, many imprint methylation errors also lead to the occurrence of various cancers (Okamoto *et al.*, 1997; Cui *et al.*, 1998). Further molecular studies will be required to understand the pathogenesis of these associations, and also to identify preventative methods to reduce the risk of occurrence of these syndromes following ART.

Supplementary data

Supplementary data are available at http://humrep.oxfordjournals.org/.

Acknowledgements

The authors thank the patients and their families who participated in this study. We are also grateful to the physicians who responded to the first and second surveys. We would like to thank Ms Chizuru Abe for technical assistance.

Authors' roles

H.H., H.O., N.M., F.S. and A.S. performed the DNA methylation analyses. M.K., K.N. and H.S. collected the samples of the patients. K.N. did the statistical analyses. H.H., M.V.D.P., R.M.J. and T.A. wrote this manuscript. All authors have read and approved the final manuscript.

Funding

This work was supported by Grants-in-Aid from the Ministry of Health, Labour and Welfare of the Japanese government (The Specified Disease Treatment Research Program; 162, 054) and Scientific Research (KAKENHI; 21028003, 23013003, 23390385), as well as the Uehara Memorial Foundation and Takeda Science Foundation (TA).

Conflict of interest

None declared.

References

Azzi S, Rossignol S, Le Bouc Y, Netchine I. Lessons from imprinted multilocus loss of methylation in human syndromes: A step toward understanding the mechanisms underlying these complex diseases. *Epigenetics* 2010;**5**:373–377.

Bliek J, Terhal P, van den Bogaard MJ, Maas S, Hamel B, Salieb-Beugelaar G, Simon M, Letteboer T, van der Smagt J, Kroes H *et al.* Hypomethylation of the H19 gene causes not only Silver-Russell syndrome (SRS) but also isolated asymmetry or an SRS-like phenotype. *Am J Hum Genet* 2006;**78**:604–614.

Bliek J, Verde G, Callaway J, Maas SM, De Crescenzo A, Sparago A, Cerrato F, Russo S, Ferraiuolo S, Rinaldi MM *et al.* Hypomethylation at multiple maternally methylated imprinted regions including PLAGL1 and GNAS loci in Beckwith-Wiedemann syndrome. *Eur J Hum Genet* 2009;**17**:611–619.

Bowdin S, Allen C, Kirby G, Brueton L, Afnan M, Barratt C, Kirkman-Brown J, Harrison R, Maher ER, Reardon W. A survey of assisted reproductive technology births and imprinting disorders. *Hum Reprod* 2007;**22**:3237–3240.

Chang AS, Moley KH, Wangler M, Feinberg AP, Debaun MR. Association between Beckwith-Wiedemann syndrome and assisted reproductive technology: a case series of 19 patients. *Fertil Steril* 2005;**83**:349–354.